Assessment of the European climate projections as simulated by the large EURO-CORDEX regional and global climate model ensemble

Erika Coppola[1], Rita Nogherotto[1], James M. Ciarlò[1], Filippo Giorgi[1], Erik van Meijgaard[2], Nikolay Kadygrov[3] , Carley Iles[3], Lola Corre[4], Marit Sandstad[5], Samuel Somot[6], Pierre Nabat[6], Robert Vautard[3], Guillaume Levavasseur[3], Clemens Schwingshackl[5], Jana Sillmann[5], Erik Kjellström[7], Grigory Nikulin[7], Emma Aalbers[2], Geert Lenderink[2], Ole B. Christensen[8], Fredrik Boberg[8], Silje Lund Sørland[9], Marie-Estelle Demory[9], Katharina Bülow[10], Claas Teichmann[10], Kirsten Warrach-Sagi[11], Volker Wulfmeyer[11]

[1] The Abdus Salam International Center for Theoretical Physic (ICTP), Strada Costiera 11, 34135 Trieste, Italy

[2] Royal Netherlands Meteorological Institute (KNMI), 3730 GA De Bilt, the Netherlands

[3] Laboratoire des Sciences du Climat et de l'Environnement, Institut Pierre-Simon Laplace (IPSL), Gif sur Yvette, France

[4]Meteo-France (42 avenue Coriolis 31057 Toulouse FRANCE)

[5] Center for International Climate Research (CICERO), Gaustadalleén 21, 0349 Oslo, Norway

[6]CNRM, Université de Toulouse, Meteo-France, CNRS, Toulouse, France, 42 avenue Coriolis 31057 Toulouse FRANCE

[7]Swedish Meteorological and Hydrological Institute, SE 60176 Norrköping, Sweden

[8]Danish Meteorological Institute, Lyngbyvej 100 - 2100 Copenhagen Ø - Denmark.

[9]Institute for Atmospheric and Climate Science, ETH Zurich, Universitätstrasse 16, 9092 Zürich, Switzerland

[10]The Climate Service Center Germany (GERICS), Chilehaus - Eingang B Fischertwiete 1, 20095 Hamburg Germany

[11]The University of Hohenheim, Schloß Hohenheim 1, 70599 Stuttgart, Germany

Corresponding author: Erika Coppola (coppolae@ictp.it)

Key Points:

- This paper presents the first of this size regional climate model ensemble to investigate and understand the climate change response over the whole Europe
- The paper confirms previous findings for mean and extreme climate change but is able to show the added value information of the high-resolution regional ensemble
- The paper assesses the regional and global model consensus in the projection and presents also the uncertainty of the signal.

Abstract

This paper analyzes the ensemble of regional climate model (RCM) projections for Europe completed within the EURO-CORDEX project. Projections are available for the two greenhouse gas concentration scenarios RCP2.6 (22 members) and RCP8.5 (55 members) at 0.11 degree resolution from 11 RCMs driven by 8 global climate models (GCMs). The RCM ensemble results are compared with the driving CMIP5 global models but also with a subset of available last generation CMIP6 projections. Maximum warming is projected by all ensembles in Northern Europe in winter, along with a maximum precipitation increase there; in summer, maximum warming occurs in the Mediterranean and Southern European regions associated with a maximum precipitation decrease. The CMIP6 ensemble shows the largest signals, both for temperature and precipitation, along with the largest inter-model spread. There is a high model consensus across the ensembles on an increase of extreme precipitation and drought frequency in the Mediterranean region. Extreme temperature indices show an increase of heat extremes and decrease of cold extremes, with CMIP6 showing the highest values and EURO-CORDEX the

finest spatial details. This dataset of unprecedented size and quality will provide the basis for impact assessment and climate service activities for the European region.

1 Introduction

Despite decades of efforts, the characterization of future climate evolutions at regional to local scales over Europe remains an open challenge which requires: (1) a large ensemble to cover all uncertainty sources (Hawkins and Sutton, 2009; Deser et al., 2012) and to explore all potential future conditions; (2) a high-resolution description of regional climate phenomena that can locally modify the climate change signal, for example due to islands, cities, and coastal or mountain areas (e.g. Giorgi et al., 2016). So far, achieving both aspects in the same modelling exercise has been impossible mostly due to limitations in computer power and international coordination. Typically, successive CMIP (Coupled Model Intercomparison Project) initiatives based on Global Climate Models (GCMs) have been able to provide large ensembles that cover reasonably well the various uncertainty sources but at too coarse spatial and temporal resolution to describe climate at regional to local scales. On the other hand, projects based on high resolution Regional Climate Models (RCMs), such as PRUDENCE (Christensen and Christensen, 2007), ENSEMBLES (Hewitt & Griggs, 2004; van der Linden and Mitchell, 2009), Med-CORDEX (Ruti et al., 2016; Somot et al., 2018) or EURO-CORDEX (Jacob et al., 2014), have not been able to reach an ensemble size which would cover sufficiently well the uncertainty range in future climate projections. For example, the PRUDENCE ensemble was mostly based on one driving GCM, the ENSEMBLES ensemble focused on one scenario and was limited to about 20 simulations (Déqué et al., 2012; Kjellström et al., 2013; Vautard et al., 2014), and early EURO-CORDEX-based studies at 12 km spatial resolution were limited to a

small ensemble size per socio-economic scenario, typically ranging from about 10 runs (Jacob et al., 2014; Tramblay & Somot, 2018) to about 20 runs (Kjellström et al., 2018).

Analyses of these previous ensembles showed some consistent signals over the European region. Both winter and summer are projected to become warmer throughout Europe, with the warming being strongest in winter over Northern Europe and in summer over the Mediterranean and northernmost Scandinavia close to the Arctic (Christensen et al., 2019; Jacob et al., 2014, Kjellström et al., 2018; Giorgi & Lionello, 2008). Extreme warm events are projected to increase, along with a higher number of heatwaves across Europe (Kjellström et al., 2018; Jacob et al., 2014; Russo et al., 2015) and substantial increasing trends in various heat stress indicators. Conversely, extreme cold events in winter are projected to decrease in frequency and intensity (Vautard et al., 2014).

Some consistent precipitation change signals have also been found. Seasonal precipitation total is projected to increase during winter in the northern half of Europe, while its change signal is more uncertain in the south. In summer, projections show a substantial decrease of precipitation over most of central and southern Europe, with a maximum in the Western Mediterranean basin, and over Spain and France, while a small increase is projected for the Scandinavian region. In fact, the Mediterranean region was identified as a climate change drought hot spot by Giorgi (2006), Giorgi & Lionello (2008) and Mora et al., (2018), while Ruosteenoja et al., (2018) showed an increased probability of drought in the Mediterranean based on soil moisture and Giorgi et al., (2018) and Spinoni et al., (2014, 2019) reached the same conclusions using precipitation deficit indices. Independent of the scenario and the temporal horizon, the precipitation change zero line

crosses continental Europe with a substantial uncertainty concerning its position (Giorgi & Coppola 2007; Jacob et al. 2014, Kjellström et al. 2018). Extreme precipitation is projected to increase throughout the entire European territory, although with a less certain signal in the southernmost Mediterranean basin (Jacob et al., 2014; Rajczak & Schär, 2017; Tramblay & Somot, 2018; Hodnebrog et al., 2019).

Recently, the EURO-CORDEX projection ensemble has been enhanced as part of the European Copernicus Climate Change Service (C3S), resulting in a high resolution (0.11 degrees) ensemble of unprecedented size. This offers the opportunity, on the one hand, to have a more thorough validation of observed climate statistics (Vautard et al., 2014; Vautard et al., 2020; Kotlarski et al., 2014) and past climate trends (Nabat et al., 2014; Christensen et al., 2019) and, on the other hand, to produce a more robust assessment of climate change projections over the European region and in particular a better characterization of uncertainties associated with mean signals. Here, the climate change signal will be characterized for temperature and heat-related indices, along with precipitation and wet and dry indices relevant for climate hazard assessment and solar radiation reaching the surface. We present both high resolution maps of changes in these indices and results aggregated over the 3 European sub-regions defined in Iturbide et al., (2020).

The second aim of the paper is to measure the degree of consistency between the EURO-CORDEX 12-km resolution large ensemble and its driving-GCM ensemble, which is a sub-sample of the CMIP5 ensemble. Finally, we also assess the first set of available CMIP6 GCMs in order to illustrate how the higher climate change sensitivity and stronger warming found in the CMIP6 GCMs (Forster et al., 2020) is translated at the European scale. The ensembles and

129 indices considered in this paper are described in section 2, while results are discussed in section
130 3 and discussion and conclusions presented in section 4.

131

132 **2 Data and Methods**

133

134 **Multimodel Ensembles of Climate Projections**

135 The regional climate projection ensemble includes 55 scenario simulations for the RCP8.5 and
136 RCP2.6 scenarios at 0.11 degree resolution over the common EURO-CORDEX domain using
137 eight driving GCMs and eleven RCMs. The details about model availability for each of the
138 variables and indices for both the RCP8.5 and RCP2.6 scenarios are reported in Table 1.

139

140 The reader is also referred to Vautard et al., (2020) for model references. Also note that not all
141 variables are available for all models, especially in the RCP2.6 projections. The second ensemble
142 used for comparison consists of 12 GCM simulations (with 8 different GCMs) from CMIP5
143 (Taylor et al., 2012). These are limited to those simulations used as boundary conditions for the
144 RCM ensemble assessed here (see Table 2). As a third ensemble, 12 simulations from CMIP6
145 (Eyring et al., 2016) are analyzed and intercompared over the European area.

146
147

148 The CMIP6 ensemble is reported in Table 3 and is based on the availability of data on the Earth
149 System Grid Federation (ESGF) archive at the time when the analysis was completed. EURO-
150 CORDEX and CMIP5 simulations share the same forcing scenarios, i.e. RCP8.5 and RCP2.6
151 (Representative Concentration Pathway; see Moss et al., 2010) while the CMIP6 simulations use
152 the SSP126 and SSP585 scenarios (Shared Socio-Economic Pathways, Riahi et al., 2017). The

time slices used to compute the climate change signal with respect to the historical period 1981-2010 are 2041-2070 for the mid-future and 2071-2100 for the far-future (end of century). The EURO-CORDEX ensemble results are presented on a regular 0.11° grid, the CMIP5 GCMs on a 2° grid and the CMIP6 on a 1° grid. These grids were chosen to be representative of the resolution of each ensemble. The robustness of the simulated changes of the three ensembles was evaluated by means of a significance test based on the dependent samples of a two-sided Student's t-test.

Extreme and impact-oriented climate indices

As in Vautard et al., (2020), we use here a set of 13 extreme and impact-oriented indices described in Table 4, which characterize a number of potential influences on different sectors. The description of the indices is provided in Vautard et al., (2020) and references therein, to which we refer for more detailed information. However, a few additional indices are used here: the Simple Daily Intensity Index (SDII) and the Highest 5-days precipitation amount (RX5day). Only for the daily WBGT index, data are bias-corrected for each climate model on each grid point and each month of the year individually using the quantile delta mapping approach described by Cannon et al., (2015). We use ERA5 as reference dataset and 1981-2010 as reference period.

4 Results

Here climate change signals are compared for the mid century (2041-2070) and end of century (or far future, 2071-2100) time slices under the RCP8.5 scenario. An identical analysis is reported for the RCP2.6 scenario for the box plot results and in the supplementary material for

the remaining analysis. The mean seasonal changes are shown for mean, maximum and minimum temperature and precipitation over the whole European domain and box plots are used to summarize the results for the Northern European (NEU), Central European (CEU) and Mediterranean (MED) regions, following the definition in Iturbide et al., (2020). Values of change are shown for the median, the 25^{th}, and 75^{th} percentiles, together with the 5^{th} and 95^{th} percentiles. Similarly, all the temperature and heat indices as well as the wet and dry indicators and radiation are shown as spatial change plots over Europe, while box plots are provided for the hazard indices.

3.1 Mean Temperature

Figure 1 shows the seasonal mean temperature change for DJF (winter) and JJA (summer), the mid and far future time slices in the RCP8.5 projections and the EURO-CORDEX, CMIP5 and CMIP6 ensembles.

In DJF all three ensembles show the well-known temperature change gradient, with the largest warming in the north and northeast and the weakest warming in the southwest and over the Atlantic. This warming pattern is to a large extent a result of the Arctic amplification related to sea-ice loss as well as the reduction of continental snow cover over vast northern areas leading to the snow albedo feedback. This figure also shows differences between the ensembles in the amplitude of the change. In general, the CMIP6 ensemble shows a much stronger warming compared to the other two CMIP5-based ensembles, except for some areas over the Atlantic in winter. Another difference relates to the RCM ensemble which, in addition to more fine-scale details, shows weaker warming over large parts of the continent compared to the driving CMIP5-GCMs. This is in line, for example, with results from Sørland et al., (2018).

Figure 2 shows the box plot for the NEU and CEU regions of the area average change for each ensemble with colored bars representing the model spread between the 25th and 75th percentiles, while the black bars indicate the 5th, 50th and 95th percentiles A projected median warming in winter of 4.5(2.5) °C is found for the RCM and CMIP5 ensemble in the far (mid) future time slices, respectively, reaching values of 6(3.5) and 5.5(3.8) °C for CMIP6. Over the MED region a smaller DJF warming is projected, with slightly less than 3.5(2) °C, for both EURO-CORDEX and CMIP5, and 4.5(2.5) °C and 6(4) °C for CMIP6. The projections for the 90% interval (range between the 5th and 95th percentile) are generally less than 1.5 degrees for the EURO-CORDEX and CMIP5 ensembles in all regions, and reach ~3 degrees in NEU and MED for CMIP6.

The JJA warming has its maximum signal over the Mediterranean land regions with values above 4(2.5), 4.5(2.5) and 6.5(3.5) °C for RCM, CMIP5 and CMIP6 respectively in the far(mid) future (Fig. 2). This result, which is in line with previous analyses (e.g. Giorgi & Lionello 2008; Giorgi & Coppola 2010) is likely connected with a marked decrease in spring and summer precipitation (as shown on Fig. 3), increased soil drying and decreased cloud cover.

The NEU and CEU regions warm less in summer, with values in the far(mid) future of 3.5(2), 3.6(2.3) 5.8(3) and 3.5(2), 4(2.3) and 6(3.4) °C respectively for the EURO-CORDEX, CMIP5 and CMIP6 ensemble. The spread connected to the projections is lower for the first two ensembles compared to the CMIP6. The RCP2.6 scenario has a general warming between 1 and 2.5 °C for both seasons and for the three ensembles, with CMIP6 being at the upper end of the distribution. In summary, the warming projected by the EURO-CORDEX ensemble is comparable with that in the CMIP5 ensemble in DJF, while it is about 0.5 degree lower on average in JJA.

These findings confirm previous results based on a more sophisticated ANOVA analysis (Déqué et al., 2007; Evin et al., 2019; Christensen et al., 2020) from which most of the temperature change signal is largely influenced by the choice of GCM, while the RCM mostly dominates the change pattern in regions of complex topography, sea-ice, soil moisture or snow. The difference between the RCM and GCM warming during summer also confirms the finding of Sørland et al., (2018) and Boé et al., (2020), i.e. that CMIP5 GCMs warm notably more than RCMs even on a pair by pair basis (not shown). Possible explanations for this result are multiple. Some studies have at least partially attributed it to the lack of aerosol forcing in the RCMs, since aerosol concentrations over Europe are expected to decrease in the future as a result of stricter emission control measures (Boé et al., 2020; Gutiérrez et al., 2020; Nabat et al., 2020). Other reasons can be related to clouds (Bartok et al., 2017) or differences in the representation of plant physiological effects (Schwingshackl et al., 2019). The consistently higher warming values of the CMIP6 ensemble, along with the much higher uncertainty spread, is in line with the higher equilibrium climate sensitivity (ECS) of some of the members of CMIP6 (Forster et al., 2020, Zelinka et al., 2020), whose origin remains unclear and is under investigation.

Maximum (TXx) and minimum (TNn) temperature seasonal projections are shown in Figures 3 and 4, while the median and percentile values are reported as box plots in Figure 2. Both variables show a similar behaviour as the mean temperature. Maximum winter warming occurs in the NEU and CEU regions, with a change of the TXx median value of about 4(2.5) $^{\circ}$C (EURO-CORDEX and CMIP5) and 5.3(3-3.5) $^{\circ}$C (CMIP6) at the far(mid) of century. In winter, TNn shows greater warming in NEU and CEU compared to TNx about 4.5(2.5) °C for EURO-CORDEX and CMIP5 and 7(4) $^{\circ}$C 5.5(4.5) $^{\circ}$C for CMIP6 far(mid) of century, probably due to

the snow albedo feedback. For the MED region, the TXx and TNx warming in DJF has values of 3.5(2) °C for the RCM and CMIP5 ensembles and 4.5(2.5) °C for the CMIP6 ensemble far(mid) of century time slice, with a very limited model spread (about 1 degree) for all the 3 ensembles probably due to the lower temperature variability over the ocean compared to the land. In summer, the changes in maximum and minimum temperature in the 3 European sub-regions have similar values (Fig. 2). For NEU the median change value for both variables by the far(mid) of 2100 are around 3.5(2) $^{\circ}$C for EURO-CORDEX and CMIP5 and 6(3) $^{\circ}$C for CMIP6; TNn for CEU has a 3.5(2)$^{\circ}$C median increase for the regional ensemble, while the GCM ensembles show stronger warming by 1(0.5) degree for CMIP5 and 2 degrees for CMIP6 for the far(mid) of century time slice. TXx shows the same behavior. In the MED region, TXx warms by about 0.5 degrees more than TNn, with median values of 4.5(2.5), 5(2.7) and 6.5(3.7) $^{\circ}$C for CORDEX, CMIP5 and CMIP6 by the far(mid) future, respectively.

3.2 Mean Precipitation

Figure 5 shows the seasonal mean precipitation change in percent of reference values for DJF and JJA. The well-known North-South dipole is evident, with positive changes in the northern part of the domain and negative changes in the southern part. The zero-change line is positioned in the southernmost location during winter over the Pyrenees, Alpine and Balkan Mountains, and shifts northward during the spring and summer season when it reaches the northernmost position placed over central eastern Europe and southern Scandinavia (Giorgi & Coppola 2007).

For NEU and CEU in DJF, the EURO-CORDEX ensemble shows a median precipitation increase for the 2071-2100(2041-2070) time slice of 15(5) % and 20(10) %, respectively, with the smallest inter-model spread for the NEU and the largest over the CEU in all ensembles (see

Fig. 2). Change patterns are similar in the CMIP5 ensemble, with an amplitude of the spread about doubled over NEU and halved over CEU compared to the EURO-CORDEX one. The CMIP6 ensemble exhibits a 25(15) % and 22(12) % median value of increase over the two regions, respectively, and a spread similar to the CMIP5 one in NEU but greater in CEU, and lower than the RCM spread. In the Mediterranean region the three ensembles project a median negative DJF precipitation change slightly above 10(5) %, with a wider spread for the RCMs.

For the summer, over the NEU the three ensembles project an increase of about 5% for both the mid and far future time slices and for both the RCP8.5 and RCP2.6 scenarios, with a larger spread for the far future time slice compared to the mid of century one and a range of 20% between the 5th and 95th percentile. Again, the RCM ensemble shows the widest spread. In CEU and MED all ensembles agree on negative changes of precipitation for far(mid) of century, spanning the range of -7(4) % for EURO-CORDEX to -20(-10) % for CMIP6 over CEU and from -22(-10) % to -32(-20) % in the Mediterranean. In all cases the CMIP5 ensemble has intermediate values between the EURO-CORDEX and CMIP6 ones. For the MED region far future projections, the range between the 5th and 95th percentile is roughly 40% in the RCM ensemble and slightly lower (35%) for both CMIP ensembles.

3.3 Temperature indices

Hot extremes

Extremely hot days, as characterized by a daily maximum temperature larger than 35°C or 40°C, have a well-marked increasing frequency for RCP8.5/SSP585, particularly in regions where their occurrence is already significant in the reference period (see Vautard et al., 2020). In Southern Spain and low-lying areas of Italy and the Balkans, the number of days (35°C / 40°C) is robustly projected to increase by more than 30 days / 10 days in the mid century and 50 days / 20 days for

294 the end of the century (Fig. 6). This may have important impacts on agriculture and health, as
295 these are typical critical thresholds above which these sectors are impacted.
296
297
298 *Wet Bulb Globe Temperature (WBGT)*
299 Humid heat, as characterized by the WBGT index, is projected to increase in large parts of
300 Europe as indicated by the number of days during which WBGT exceeds 31°C, a danger
301 threshold for which impacts and reduction of productivity are expected for outdoor activities
302 (Fig. 6). The EURO-CORDEX ensemble shows an increase of more than 30 days in low-lying,
303 coastal or near-coastal areas of Southern Europe (e.g. Andalucia, Po Valley, lower Rhone and
304 Garonne Valleys, coastal areas of Greece and Turkey, plains near the Black Sea). The number of
305 days above the danger threshold is projected to almost double in the far future projection. (see
306 Vautard et al., 2020). In contrast to EURO-CORDEX, the WBGT signal is spread throughout
307 Europe much more evenly in CMIP5 and CMIP6, highlighting the beneficial effects of improved
308 orography resolution in RCM simulations compared to GCMs. The patterns in CMIP5 and
309 CMIP6 are consistent, both showing large increases of the number of days with WBGT
310 exceeding 31°C. Note that WBGT exceedances exhibit a cold bias in RCMs for current climate
311 conditions (Vautard et al., 2020) and absolute changes in the number of days with WBGT
312 exceeding 31°C should thus be treated cautiously.
313
314 *Cooling degree days >22 °C*
315 Cooling degree days, which measure the energy demand for cooling are projected to strongly
316 increase in several European regions. For the southernmost Mediterranean areas, we note
317 approximately a doubling of the number of CDDs by the mid century and tripling by the end of

the century compared to the present-day reference value (see Vautard et al., 2020), with a large spread among the ensembles (EURO-CORDEX showing lower values than CMIP5 and CMIP6). Again, we note that CMIP5 and CMIP6 exhibit reduced regional orographic details than EURO-CORDEX. Large increases in CDD are also expected by the end of century in Central Europe, while Scandinavia only shows a limited increase.

Growing degree days > 5°C and Length of Frost-Free Period

The GDD index, which is linked to plant phenology and growing season length, is projected to increase across Europe, with a North-South gradient and significant differences between the ensembles. EURO-CORDEX and CMIP5 have a consistent change signal, while CMIP6 has a signal about 1.5 times larger than CMIP5. The GDD index is sensitive to spring and summer temperatures, and therefore its pattern is correlated to the temperature change pattern in these seasons.

By contrast, the LFFP index, which is mostly sensitive to winter temperature changes, has a different change pattern. It increases more in Northern Europe (40-70 days for mid century and 60-100 days for the end of century) than in Southern Europe (15-30 days and 20-40 days) for RCP8.5, with a rather homogeneous spatial pattern, except in a few scattered areas such as along southwestern coasts of the Iberian Peninsula where frost days are almost absent. Again, the EURO-CORDEX and CMIP5 ensembles show rather similar changes while CMIP6 gives a larger increase. Note that, along the coastlines, the GCMs may be inaccurate and mix sea temperatures with land temperatures into a smoother pattern, hence the smaller increase.

Frost days

Frost days relevant for both agriculture and energy, are projected to become much less frequent in the RCP8.5 Scenario. Their number varies in the reference period from about 150-250 days in Northern Europe to almost none in South-Western Europe (see Vautard et al., 2020). For RCP8.5, in the mid century, the decrease in frost days number is about 20-40 days (with a doubled reduction in CMIP6 in Northern and Central Europe), and at the end of the century, frost days are reduced by 50-60 days.

3.4 Wet and Dry extremes

Precipitation 99th percentile, SDII, RX1day, RX5day

Figure 7 shows the extreme precipitation indices P99 (often connected with the pluvial flooding hazard), RX1day, RX5day and the precipitation intensity index SDII for the mid and far future time slices in the RCP8.5 scenario. All 3 indices for all the RCM and GCM ensembles show an increase in extreme precipitation events, with a maximum by the far(mid) of century above the 20(10) % median increase over the European continental region and Scandinavia (Fig. 9 box plot). The most intense changes are shown by the EURO-CORDEX ensemble over the CEU and MED regions, while the CMIP6 ensemble shows the largest increases in the north east uppermost corner of the NEU region.

The Rx1day extreme index exhibits the strongest positive change among the 3 indices, with only less than 5% non-significant negative changes limited to the Gibraltar Strait, Pyrenees, Morocco

coasts and the Peloponnesus in Greece. Due to the higher resolution, the EURO-CORDEX ensemble indicates a pronounced increase in extreme 1day precipitation over the Padania plain in Italy and in Tuscany. The land sea contrast is quite evident between the Tyrrhenian and Adriatic seas and the Italian peninsula, with more extreme values over the ocean and in particular a maximum over the northernmost part of the Adriatic Sea where the Venice lagoon is located.

A minimum of the daily maximum precipitation increase (RX1day) is evident over all the European mountains, such as the Pyrenees, the Alps, the Apennines, the Carpathians and the Norwegian mountains, and a maximum along the UK and Ireland western coasts, Northern France and Germany. The same characteristics are also evident in the P99, RX5day and SDII indices, although for the later the signal is somehow more damped. All these small-scale features are not resolved in the GCM change plots due to the coarser resolution which does not allow the GCMs to adequately resolve orographically forced circulation dynamical and thermodynamical effects and land surface feedback (Chan et al., 2014; Giorgi et al. 2016). The EURO-CORDEX projections have in general a wider spread for both the mid and far future time slices followed by CMIP5 and CMIP6, except for the NEU region where the CMIP6 have the highest projection uncertainty.

Drought frequency change per decade (DF) and Consecutive Dry Day (CDD)

The mean annual CCD and the DF change are shown in Figure 8 for two time slices and for all ensembles. For both indices a significant maximum is observed over the Mediterranean region with the CDD being positive everywhere and the DF showing the well-known north-south dipole structure (Spinoni et al., 2014), i.e. an increase of number of droughts in the south and a decrease in the uppermost north east European areas and Scandinavia. The CDD spatial structure is quite

similar among the three ensembles, with the CMIP6 having longer dry spells for a broader region covering the whole Mediterranean Sea up to the southwestern French coasts and the Alps. An increase in the number of droughts per decade in the Mediterranean is projected by all model ensembles, with a median value of 3(1.8) for the RCM ensemble, 3.5(2) for CMIP5 and 4(2.5) for the CMIP6 ensemble by the far(mid) of century (Fig. 9 box plot). The projection uncertainties are quite small (between 1 and 2 events per decade) as shown by the CMIP6 and EURO-CORDEX ensembles, respectively. Also, in the NEU region the three ensembles show a consistent (low uncertainty) decrease of the number of droughts between 1 and 2 events per decade by the end of century or around 1 event for the mid century. The most uncertain region is the CEU, where the zero line is positioned, with a pronounced latitudinal difference between the RCM and CMIP6 ensembles. The EURO-CORDEX ensemble has the zero-line placed in the southernmost location, going from the UK through Germany, Austria and the Balkans; the CMIP6 has the line just over southern Sweden and the Baltic sea, while the CMIP5 zero line lies in between. This uncertainty is reflected in the box plot of Figure 9, where median values spanning from negative to positive are reported when moving from the regional model ensemble to the CMIP6 ensemble (CMIP5 is positioned around the zero change values) for all the time slices.

3.1.4 Simulated changes for downward surface shortwave radiation (W/m2)

Figure 11 shows the change signal for the mid- and far-future periods for the Surface Downwelling Shortwave Radiation (rsds) in both scenarios and ensembles.

The common behavior to all ensembles is a tripole pattern, with an increase in rsds over the Mediterranean area and Central Europe and a decrease in Northern Europe and the extreme South of the domain over the Sahara regions. This tripole is likely due to a tripole-like pattern in cloud cover change. Local values reach up to -10 W/m^2 over North-Eastern Europe and more than +15 W/m2 over the Balkans and South-Eastern Europe. Note, however, that this tripole pattern is less visible in the CMIP6 ensemble for which the northern pole nearly disappears and the median change over the NEU zone is positive (see Fig. 12). For the EURO-CORDEX RCMs and CMIP5 GCMs, the values and spatial patterns obtained in Figures 11 and 12 are in line with previous studies (Bartok et al., 2017; 2019 Gutiérrez et al.; 2020; Boé et al., 2020).

An important feature of Figures 11 and 12 is the strong difference between the change signals of the three model ensembles over Central Europe, where the EURO-CORDEX ensemble median values show a decrease in the shortwave radiation reaching the surface for CEU and both periods, whereas both CMIP ensembles show a large increase. This is one of the rare cases of GCM-RCM inconsistency in the climate change response at large scale and confirms the results obtained with CMIP5 and EURO-CORDEX smaller ensembles by Bartok et al., (2017), Boé et al. (2020), Gutiérrez et al., (2020) and Nabat et al. (2020). It has been recently attributed to the different way aerosols are represented currently in GCMs and RCMs (Gutiérrez et al., 2020). In addition, Bartok et al., (2017) showed that cloud cover trends behave very differently in CMIP5 GCMs and EURO-CORDEX RCMs, with a decreasing cloud cover trend in GCMs and an absence of trends in RCMs.

To our knowledge, what differs most between RCMs and GCMs is the temporal evolution of the aerosol forcing (a general decrease of the aerosol load over continental Europe during the scenario period), which is taken into account in CMIP5 and CMIP6 despite large uncertainties,

whereas it is not taken into account in most of the EURO-CORDEX RCMs. More specifically, only three RCMs (RACMO22E, ALADIN53 and ALADIN63) apply evolving aerosol forcing in the future, resulting in only 11 runs out of 55 for RCP85 and 5 out of 22 for RCP26.

Looking at individual RCM future responses, for example for the RCP8.5 and the near-future, we note a strong increase (maximum value of +20 W/m2) over Central Europe and the Mediterranean for the ALADIN and RACMO22E runs regardless of the versions used and the driving GCM, along with a negative or weakly positive signal for all other RCMs, except for one of the RegCM4-6 runs (not shown). Plotting multi-model mean values for the RCM ensemble in Figure 11 therefore gives a large weight to RCMs without evolving aerosols. Note that the GCM-RCM discrepancy in rsds change also have implications when computing potential photovoltaic production in Europe (Gutiérrez et al., 2020).

It is also worth noting that the change response is largely stronger in CMIP6 than in CMIP5 models. Moreover, the choice of the socio-economic scenario and of the temporal horizon have weak impacts on the results. For example, for the end of the 21st century and the RCP2.6 and SSP126 scenarios, CMIP5 GCMs project an increase by +4 W/m2 (median value) for the CEU region whereas CMIP6 GCMs project an increase by +7.5 W/m2 and CORDEX RCMs a decrease by -2 W/m2. The uncertainty in the future change of surface shortwave radiation is thus dominated by the choice of the model ensemble. Concerning the surface radiation change signal over the European seas, on average the EURO-CORDEX ensemble projects a decrease in surface shortwave radiation over the Baltic and North Seas and a close-to-zero change for the Mediterranean and Black Seas, whatever the scenario and the temporal horizon. Conversely, the CMIP5 ensemble projects nearly no change for the Baltic and North Seas and an increase for the Mediterranean and Black Seas, whereas the CMIP6 ensemble projects a clear and strong increase

for all European Seas. These differences in the radiation change signal over the European Seas could have strong impacts on the regional sea physics and marine biogeochemistry scenario simulations, often driven by or coupled to Atmosphere-RCMs (Darmaraki et al., 2019; Soto-Navarro et al., 2020; Gröger et al., 2019). An interesting small-scale feature in the radiation change pattern is the specific signal obtained over the Alps with the CORDEX ensemble for the RCP8.5. Contrary to the GCMs, the RCMs simulate a contrast of response between the Alps (strong decrease in surface shortwave radiation) and the surrounding areas (weak signal or increase). This interesting contrast could be the signature of a potential local added-value of the RCMs in future climate response as already shown for summer precipitation by Giorgi et al., (2016). It remains unexplained so far but could be linked to a stronger response of cloud cover over the Alps or to a locally lower influence of the aerosol load decrease.

5 Conclusions

In this paper, we investigate and characterize the climate change response over the whole European domain derived from the EURO-CORDEX RCM, and CMIP5 and CMIP6 GCM sub-ensembles for two different scenarios (SSP585 or RCP8.5) and (SSP126 or RCP2.6), a far, and a mid future time slice. The RCM projections are compared with the driving CMIP5 GCM projections and the consistency of the corresponding signals is analyzed. All the results are also put in the context of the new CMIP6 projections, which show a stronger warming signal than CMIP5 partly related to the higher ECS in several of the models compared to the previous generation GCMs.

For the mean European climate, the well-known south-north seasonal gradients in temperature and precipitation are projected, with maximum warming and increase in precipitation in the

northern regions in winter and maximum warming and a significant decrease in precipitation in the southern regions in summer and in particular over the Mediterranean basin. These results confirm previous findings from early regional ensembles such as PRUDENCE and ENSEMBLE, but are able to add a better quantification of the uncertainty and robustness due to the increased size of the present ensemble.

In both summer and winter, stronger warming and precipitation responses are always shown by the CMIP6 ensemble. Conversely the EURO-CORDEX ensemble shows the least pronounced warming and precipitation responses. The higher resolution of the RCM ensemble allows for a more detailed description of the warming and precipitation change patterns, showing for example higher warming and precipitation responses over mountainous regions, and a much more detailed land-sea contrast along the Mediterranean, Baltic sea and Norwegian coasts and islands.

The mean, maximum and minimum temperature projection spread in all seasons and regions is much lower in the EURO-CORDEX and CMIP5 ensembles (almost half the magnitude) than in the CMIP6 one. The mean precipitation spread is comparable for all the ensembles and is smallest in northern and central Europe in winter and northern Europe in summer.

All the projections agree on an increase of extreme precipitation over the Northern and Central European regions for all selected indices. The results over the Mediterranean region are more contrasted, with some indices showing no clear trend or even a decrease. For extreme precipitation, the EURO-CORDEX ensemble shows higher maxima together with fine scale and accurate spatial placement of the signal, for example minima over the highest elevations and maxima over the Adriatic, Tyrrhenian and Baltic seas. For extreme precipitation the inter-model agreement is high in terms of the direction of the changes and the model spread is limited to about 10% in northern and central Europe and to less than 15% in the Mediterranean. There is a

consensus across models on a small but significant (almost everywhere) change of dry spell length in north and central Europe and a positive significant change in the Mediterranean basin, confirmed by a unanimous projection of a significant increase in the number of droughts.

The quantification of the uncertainty and robustness of the projections for multiple wet and dry indicators has been presented adding to previous studies like Jacob et al., (2014) and Christensen et al., (2019) that were using a reduced size ensemble with no information on the uncertainty and fewer indices.

For the first time in a comprehensive way climate change impact on thresholds relevant for one or more particular sectors is assessed with such a dataset. These extreme and impact-oriented indices show increasing heat extremes and decreasing cold extremes. In summer, RCMs exhibit a slightly lower signal than their driving CMIP5 GCMs, which themselves exhibit a lower signal than the CMIP6 model ensemble analyzed. For extreme heat indices, the RCMs reveal details not shown by GCMs: low-lying and coastal Mediterranean areas are projected to cross severe heat stress thresholds (e.g. Wet Bulb Globe Temperature > 35°C) for up to a few weeks, conditions that are not found in current climate. Indices sensitive to winter temperatures (e.g. length of frost-free period) generally have a larger signal in Northern Europe while indices sensitive to summer temperature (e.g. Growing degree-day) have a larger signal in Southern Europe.

An overall increase in solar radiation reaching the surface is expected over the Mediterranean region and a decrease over northern Europe. However, the amplitude of these changes as well as the sign of the change over Central Europe remains uncertain and sometimes inconsistent between RCMs and GCMs, specifically in response to varying forcings such as due to aerosols which are treated differently in different models. In general, we find that the future response of

surface solar radiation in Europe is very sensitive to the choice of model ensemble and less to the choice of scenario or temporal horizon.

The EURO-CORDEX high resolution large ensemble, along with the CMIP5 and CMIP6 ones, represent an invaluable resource for climate change studies over the European region. It has been shown how this ensemble provides the basis for application to impact, vulnerability and adaptation studies over the region and for climate service activities. The size of the ensemble, unique for the EURO-CORDEX RCMs, also allows a better characterization of uncertainties in the simulated change signals, an important aspect for end-user applications. Here we presented a basic analysis of a limited set of standard variables and indices necessary to characterize the first order behavior of the projections in the various ensembles. However, a more in depth and comprehensive analysis of additional features is necessary and is indeed under way, most noticeably of changes in circulation characteristics and regimes, and will be presented in future studies.

Acknowledgments, Samples, and Data

All the data used in this work are available on the ESGF. The Earth System Grid Federation (ESGF) is an international collaboration with a current focus on serving the World Climate Research Programme's (WCRP) Coupled Model Intercomparison Project (CMIP) and supporting climate and environmental science in general. Data is searchable and available for download at the Federated ESGF-CoG Nodes https://esgf.llnl.gov/nodes.html

The work of C.S., M.S. and J.S. is funded by the European Union's Horizon 2020 research and innovation programme under grant agreement No 820655 (EXHAUSTION) and the ERANET-

SusCROP Cofund Action (RCN grant no. 299600/E50). IPSL authors thank the CEA TGCC supercomputing center for providing the computer allocation.

Part of this study has been funded by the Copernicus Climate Change Service. ECMWF implements this Service on behalf of the European Commission.

The RegCM simulations for the ICTP institute have been completed thanks to the support of the CINECA supercomputing center, Bologna, Italy.

CLMcom-CCLM-4-8-17 simulations were run on the Piz Daint supercomputer at the Swiss National Supercomputing Centre (CSCS) under project ID s432, and at the German Climate Computing Centre (DKRZ) supported by the German Federal Ministry of Education and Research (BMBF). CLMcom-ETH-COSMO-crCLIM-v1-1 simulations were run on Piz Daint at CSCS under the PRINCIPLES project. ETH acknowledges PRACE for awarding access to Piz Daint at ETH Zürich/CSCS (Switzerland). Four UHOH-WRF361H simulations were funded within the ReKliEs-De project under the grant no. 01LK140 by the BMBF and one UHOH-WRF361H simulation was funded by the German Science Foundation within the Research Unit 1695. UHOH-WRF361H simulations were run on Hazel Hen at the High Performance Computing Center in Stuttgart (HLRS).

References

Bartók, B., Wild, M., Folini, D., Lüthi, D., Kotlarski, S., Schär, C., Vautard, R. et al. (2017). Projected changes in surface solar radiation in CMIP5 global climate models and in EURO-CORDEX regional climate models for Europe. *Climate Dynamics*, *49*(7-8), 2665-2683.

Bartok, B., Tobin, I., Vautard, R., Vrac, M., Jin, X., Levavasseur, G., Denvil, et al. (2019). A climate projection dataset tailored for the European energy sector. *Climate services*, 100138.

572 Boé, J., Somot, S., Corre, L. & Nabat, P. (2020). Large differences in Summer climate change
573 over Europe as projected by global and regional climate models: causes and consequences.
574 Climate Dynamics, doi:10.1007/s00382-020-05153-1
575
576 Cannon, A. J., S. R. Sobie, & T. Q. Murdock (2015). Bias correction of GCM precipitation by
577 quantile mapping: How well do methods preserve changes in quantiles and extremes? Journal of
578 Climate, 28 (17), 6938-6959, doi:10.1175/JCLI-D-14-00754.1.
579
580 Chan, S. C., Kendon, E. J., Fowler, H. J., Blenkinsop, S., Roberts, N. M. & Ferro, C. A. T.
581 (2014). The value of high-resolution metoffice regional climate models in the simulation of
582 multihourly precipitation extremes. Journal of Climate. 276155–74
583
584 Christensen, J. H. & Christensen, O. B. (2007). A summary of the PRUDENCE model projection
585 of changes in European climate by the end of this century. Climate Change. 81:1–30
586
587 Christensen, J. H., Larsen, M. A., Christensen, O. B., Drews, M., & Stendel, M. (2019).
588 Robustness of European climate projections from dynamical downscaling. Climate Dynamics,
589 53(7-8), 4857-4869.
590
591 Darmaraki, S., Somot, S., Sevault, F., Nabat, P., Cabos, W., Cavicchia, L., Djurdjevic, V., Li, L.,
592 Sannino, G. & Sein D. (2019). Future evolution of Marine Heat Waves in the Mediterranean Sea.
593 Climate Dynamics, 53 (3-4):1371-1392, doi: 10.1007/s00382-019-04661-z
594
595 Déqué, M., Rowell, D. P., Lüthi, D., Giorgi, F., Christensen, J. H., Rockel, B., ... & van den
596 Hurk, B. J. J. M. (2007). An intercomparison of regional climate simulations for Europe:
597 assessing uncertainties in model projections. Climatic Change, 81(1), 53-70.
598
599 Déqué, M., Somot, S., Sanchez-Gomez, E., Goodess, C.M., Jacob, D., Lenderink, G. & O.B.
600 Christensen O.B. (2012). The spread amongst ENSEMBLES regional scenarios: Regional
601 Climate Models, driving General Circulation Models and interannual variability. *Climate*
602 *Dynamics*, 38(5-6), 951-964, doi: 10.1007/s00382-011-1053-x
603
604 Deser, C., Phillips, A., Bourdette, V., & Teng, H. (2012). Uncertainty in climate change
605 projections: the role of internal variability. Climate dynamics, 38(3-4), 527-546.
606
607 Drobinski, P., Ducrocq, V., Alpert, P., Anagnostou, E., Béranger, K., Borga, M., ... & Estournel,
608 C. (2014). HyMeX: A 10-year multidisciplinary program on the Mediterranean water cycle.
609 *Bulletin of the American Meteorological Society*, *95*(7), 1063-1082.
610
611 Eyring, V., Bony, S., Meehl, G. A., Senior, C. A., Stevens, B., Stouffer, R. J., & Taylor, K. E.
612 (2016). Overview of the Coupled Model Intercomparison Project Phase 6 (CMIP6) experimental
613 design and organization. Geoscientific Model Development (Online), 9 (LLNL-JRNL-736881).
614 https://doi.org/10.5194/gmd-9-1937-2016.
615

Evin, G., Hingray, B., Blanchet, J., Eckert, N., Morin, S., & Verfaillie, D. (2019). Partitioning uncertainty components of an incomplete ensemble of climate projections using data augmentation. Journal of Climate, 32(8), 2423-2440.

Field, C. B., Barros, V., Stocker, T. F., & Dahe, Q. (Eds.). (2012). Managing the risks of extreme events and disasters to advance climate change adaptation: special report of the intergovernmental panel on climate change. Cambridge University Press.

Forster, P. M., Maycock, A. C., McKenna, C. M., & Smith, C. J. (2020). Latest climate models confirm need for urgent mitigation. Nature Climate Change, doi:10.1038/s41558-019-0660-0

Giorgi, F. (2006). Climate change hot-spots. Geophysical research letters, 33(8).

Giorgi, F. & Coppola, E. (2007). The European Climate-Change Oscillation (ECO), Geophys. Res. Lett., 34, L217003, doi: 10.1029/2007GL031223

Giorgi, F., & Lionello, P. (2008). Climate change projections for the Mediterranean region. *Global and planetary change*, *63*(2-3), 90-104.

Giorgi, F., & Coppola, E. (2010). Does the model regional bias affect the projected regional climate change? An analysis of global model projections. Climatic Change, 100(3-4), 787-795.

Giorgi, F., Torma, C., Coppola, E., Ban, N., Schär, C. & Somot, S. (2016). Enhanced summer convective rainfall at Alpine high elevations in response to climate warming. *Nature Geoscience, 9, 584–589,* doi:10.1038/ngeo2761

Giorgi, F., Coppola, E., & Raffaele, F. (2018). Threatening levels of cumulative stress due to hydroclimatic extremes in the 21st century. Climate and Atmospheric Science, 1(1), 1-9.

Gröger, M., Arneborg, L., Dieterich, C., Höglund, A., & Meier, H. E. M. (2019). Summer hydrographic changes in the Baltic Sea, Kattegat and Skagerrak projected in an ensemble of climate scenarios downscaled with a coupled regional ocean–sea ice–atmosphere model. Climate Dynamics, 53(9-10), 5945-5966.

Gutiérrez, C., Somot, S., Nabat, P., Mallet, M., Corre, L., Van Meijgaard, E., Perpiñán, O. et al. (2019). Future evolution of surface solar radiation and photovoltaic potential in Europe: investigating the role of aerosols. *ERL (in rev.)*

Hawkins, E., & Sutton, R. (2009). The potential to narrow uncertainty in regional climate predictions. *Bulletin of the American Meteorological Society*, *90*(8), 1095-1108.
Hewitt CD, Griggs DJ (2004) Ensembles-based predictions of climate changes and their impacts. Eos 85:566

Hodnebrog, Ø., Myhre, G., Samset, B. H., Alterskjær, K., Andrews, T., Boucher, O & Kirkevåg, A. (2019). Water vapour adjustments and responses differ between climate drivers.

M. Iturbide, M., Gutiérrez, J.M., Alves, L., Bedia, J., Cerezo-Mota, R., Di Luca, A., Faria, S.H., Gorodetskaya, I. et al. (2020). An update of IPCC physical climate reference regions for subcontinental analysis of climate model data: Definition and aggregated datasets. Submitted to Earth System Science Data

Jacob, D., Petersen, J., Eggert, B., Alias, A., Christensen, O.B., Bouwer, L., Braun, A. et al. (2014). EURO-CORDEX: New high-resolution climate change projections for European impact research. *Regional Environmental Change, 14(2), 563-578. doi: 10.1007/s10113-013-0499-2*

Kjellström, E., Thejll, P., Rummukainen, M., Christensen, J.H., Boberg, F., Christensen, O.B. & Fox Maule, C. (2013). Emerging regional climate change signals for Europe under varying large-scale circulation conditions. Clim Res 56:103–119. https://doi.org/10.3354/cr01146.

Kjellström, E., Nikulin, G., Strandberg, G., Christensen, O.B., Jacob, D., Keuler, K., Lenderink, G. et al. (2018). European climate change at global mean temperature increases of 1.5 and 2°C above pre-industrial conditions as simulated by the EURO-CORDEX regional climate models. *Earth Syst. Dynam., 9, 459-478, 2018*, https://doi.org/10.5194/esd-9-459-2018, https://www.earth-syst-dynam-discuss.net/esd-2017-104/ . *Special Issue: The Earth system at a global warming of 1.5°C and 2.0°C*

Kotlarski, S., Keuler, K., Christensen, O. B., Colette, A., Déqué, M., Gobiet, A. & Nikulin, G. (2014). Regional climate modeling on European scales: a joint standard evaluation of the EURO-CORDEX RCM ensemble. Geoscientific Model Development, 7, 1297-1333.

McCabe, G. J., Betancourt, J. L., & Feng, S. (2015). Variability in the start, end, and length of frost-free periods across the conterminous United States during the past century. *Int. J. Climatol.* 35, 4673–4680. doi:10.1002/joc.4315.

Mora, C., Spirandelli, D., Franklin, E. C., Lynham, J., Kantar, M. B., Miles, W., ... & Barba, E. W. (2018). Broad threat to humanity from cumulative climate hazards intensified by greenhouse gas emissions. Nature Climate Change, 8(12), 1062-1071.

Moss, R. H., Edmonds, J. A., Hibbard, K. A., Manning, M. R., Rose, S. K., Van Vuuren, D. P. & Meehl, G. A. (2010). The next generation of scenarios for climate change research and assessment. Nature, 463(7282), 747-756.

Nabat, P., Somot, S., Mallet, M., Sanchez-Lorenzo, A., & Wild, M. (2014). Contribution of anthropogenic sulfate aerosols to the changing Euro-Mediterranean climate since 1980. Geophysical Research Letters, 41(15), 5605-5611.

Nabat, P., Somot, S., Cassou, C., Mallet, M., Michou, M., Bouniol, D., Decharme, B., Drugé, T. et al. (2020). Modulation of radiative aerosols effects by atmospheric circulation over the Euro-Mediterranean region, Atmos. Chem. Phys. Discuss., in review, DOI:10.5194/acp-2019-1183

Rajczak, J., & Schär, C. (2017). Projections of future precipitation extremes over Europe: A multimodel assessment of climate simulations. Journal of Geophysical Research: Atmospheres, 122(20), 10-773.

Riahi, K.; van Vuuren, D. P.; Kriegler, E.; Edmonds, J.; O'Neill, B. C.; Fujimori, S.; Bauer, N. et al. (2017). "The Shared Socioeconomic Pathways and their energy, land use, and greenhouse gas emissions implications: An overview". *Global Environmental Change*. **42**: 153–168. doi:10.1016/j.gloenvcha.2016.05.009.

Ruosteenoja, K., Räisänen, J., Venäläinen, A., & Kämäräinen, M. (2016). Projections for the duration and degree days of the thermal growing season in Europe derived from CMIP5 model output. *Int. J. Climatol.* 36, 3039–3055. doi:10.1002/joc.4535.

Ruosteenoja, K., Markkanen, T., Venäläinen, A., Räisänen, P., & Peltola, H. (2018). Seasonal soil moisture and drought occurrence in Europe in CMIP5 projections for the 21st century. Climate dynamics, 50(3-4), 1177-1192.

Russo, S., Sillmann, J. & Fischer, E. (2015). Top ten European heatwaves since 1950 and their occurrence in the coming decades, Environ. Res. Lett., 10, doi: 10.1088/1748-9326/10/12/124003.

Ruti, P. M., Somot, S., Giorgi, F., Dubois, C., Flaounas, E., Obermann, A., Dell'Aquila, A. et al. (2016). MED-CORDEX initiative for Mediterranean Climate studies. *Bull. Amer. Meteor. Soc., 97(7), 1187-1208, July 2016, doi:* http://dx.doi.org/10.1175/BAMS-D-14-00176.1.

Schwingshackl, C., Davin, E.L., Hirschi, M., Sørland, S.L., Wartenburger, R., and Seneviratne, S.I. Regional climate model projections underestimate future warming due to missing plant physiological CO2 response, Environmental Research Letters, 14, doi: 10.1088/1748-9326/ab4949.SSomot, S., Ruti, P., Ahrens, B., Coppola, E., Jordà, G., Sannino, G., Solmon, F. (2018b). Editorial for the Med-CORDEX special issue. *Clim. Dyn. 51(3):771-777, doi: 10.1007/s00382-018-4325-x, https://link.springer.com/article/10.1007/s00382-018-4325-x.*

Soto-Navarro, J., Jordà, G., Amores, A., Cabos, W., Somot, S., Sevault, F., Macías, D. et al. (2019). Evolution of Mediterranean Sea water properties under climate change scenarios in the Med-CORDEX ensemble. Clim. Dyn, 1-31. https://doi.org/10.1007/s00382-019-05105-4

Sørland, S. L., C. Schär, D. Lüthi & E. Kjellström (2018). Bias patterns and climate change signals in GCM-RCM model chains. Env. Res. Letters, 13, 074017. doi https://doi.org/10.1088/1748-9326/aacc77.

Spinoni, J., Naumann, G., Carrao, H., Barbosa, P., &and Vogt, J. (2014)., World drought frequency, duration, and severity for 1951-2010. Int. J. Climatol. 34, 2792–2804. doi:10.1002/joc.3875.

Spinoni, J., Vogt, J., &and Barbosa, P. (2015). European degree-day climatologies and trends for the period 1951-2011. Int. J. Climatol. 35, 25–36. doi:10.1002/joc.3959.

Spinoni, J., P. Barbosa, E. Bucchignani, J. Cassano, T. Cavazos, J. H. Christensen, O. B. Christensen et al. ,(2019). Future global meteorological drought hotspots: a study based on CORDEX data, Journal of Climate, https://doi.org/10.1175/JCLI-D-19-0084.1

Taylor, K.E., Stouffer, R.J. & Meehl, G.A. (2012). An Overview of CMIP5 and the Experiment Design. Bull Am Meteorol Soc 93:485–498. https://doi.org/10.1175/BAMS-D-11-00094.1

Tramblay, Y. & Somot, S. (2018). Future evolution of extreme precipitation in the Mediterranean. *Climatic Change*, *151*(2), 289-302, *https://doi.org/10.1007/s10584-018-2300-5*

Van der Linden, P. &Mitchell, J.F.B. (eds) (2009). ENSEMBLES: climate change and its impacts: summary of research and results from ENSEMBLES project. Met Office Hadley Centre, Exeter

Vautard, R., Gobiet, A., Sobolowski, S., Kjellström, E., Stegehuis, A., Watkiss, P., ... & Jacob, D. (2014). The European climate under a 2 C global warming. Environmental Research Letters, 9(3), 034006.

Vautard, R., N. Kadygrov, C. Iles, F. Boberg, E. Buonomo, K. Bülow, E. Coppola et al. (2020). Evaluation of the large EURO-CORDEX regional climate model ensemble, J. Geophys. Res., submitted.

Willett, K. M., & Sherwood, S. (2012). "Exceedance of heat index thresholds for 15 regions under a warming climate using the wet-bulb globe temperature." *International Journal of Climatology* 32.2, 161-177.

Zelinka, M. D., Myers, T. A., McCoy, D. T., Po-Chedley, S., Caldwell, P. M., Ceppi, P., et al. (2020). Causes of higher climate sensitivity in CMIP6 models. Geophysical Research Letters, 47, e2019GL085782. https:// doi.org/10.1029/2019GL085782

776
777
778
779 **Tables**
780
781 Table 1:
782 EURO-CORDEX RCMs and their corresponding driving GCM (with variant label) variable (tas
783 = atmospheric 2 meter temperature; tasmin = minimum 2 meter daily temperature; tasmax =
784 maximum 2 meter daily temperature; pr = precipitation; q = specific humidity, rsds = Surface
785 Downwelling Shortwave Radiation) used in this study. This list is relevant for all historical and
786 rcp85 and RCM2.6 simulations (☑rcp8.5, ✳=rcp2.6).
787

Driving CMIP5 GCM	**Variant**	**RCM**	**tas**	**tasmin**	**tasmax**	q	**pr**	**rsds**
CCCma-CanESM2	r1i1p1	CLMcom-CCLM4-8-17	☑	☑	☑	☑	☑	☑
CCCma-CanESM2	r1i1p1	GERICS-REMO2015	☑	☑	☑	☑	☑	☑
CNRM-CERFACS-CNRM-CM5	r1i1p1	CLMcom-CCLM4-8-17	☑	☑	☑	☑	☑	☑
CNRM-CERFACS-CNRM-CM5	r1i1p1	SMHI-RCA4	☑	☑	☑	☑	☑	☑
CNRM-CERFACS-CNRM-CM5	r1i1p1	CNRM-ALADIN53	☑✳	☑	☑	☑	☑✳	☑
CNRM-CERFACS-CNRM-CM5	r1i1p1	CNRM-ALADIN63	☑✳	☑✳	☑✳	☑✳	☑✳	☑✳
CNRM-CERFACS-CNRM-CM5	r1i1p1	KNMI-RACMO22E	☑✳	☑✳	☑✳	☑✳	☑✳	☑✳
CNRM-CERFACS-CNRM-CM5	r1i1p1	GERICS-REMO2015	☑	☑	☑	☑	☑	☑
CNRM-CERFACS-CNRM-CM5	r1i1p1	DMI-HIRHAM5	☑	☑	☑	☑	☑	☑
CNRM-CERFACS-CNRM-CM5	r1i1p1	IPSL-WRF381P	☑	☑	☑	☑	☑	☑
ICHEC-EC-EARTH	r12i1p1	CLMcom-CCLM4-8-17	☑✳	☑✳	☑✳	☑✳	☑✳	☑✳
ICHEC-EC-EARTH	r12i1p1	CLMcom-ETH-COSMO-crCLIM-v1-1	☑	☑	☑	☑	☑	☑
ICHEC-EC-EARTH	r12i1p1	DMI-HIRHAM5	☑	☑	☑	☑	☑	☑
ICHEC-EC-EARTH	r12i1p1	KNMI-RACMO22E	☑✳	☑✳	☑✳	☑✳	☑✳	☑✳

ICHEC-EC-EARTH	r12i1p1	GERICS-REMO2015	☑✲	☑✲	☑✲	☑✲	☑✲	☑✲
ICHEC-EC-EARTH	r12i1p1	UHOH-WRF361H	☑	☑	☑		☑	
ICHEC-EC-EARTH	r1i1p1	DMI-HIRHAM5	☑	☑	☑	☑	☑	☑
ICHEC-EC-EARTH	r1i1p1	KNMI-RACMO22E	☑	☑	☑	☑	☑	☑
ICHEC-EC-EARTH	r3i1p1	DMI-HIRHAM5	☑✲	☑✲	☑✲	☑✲	☑✲	☑✲
ICHEC-EC-EARTH	r3i1p1	KNMI-RACMO22E	☑	☑	☑	☑	☑	☑
ICHEC-EC-EARTH	r1i1p1	SMHI-RCA4	☑	☑	☑	☑	☑	☑
ICHEC-EC-EARTH	r12i1p1	SMHI-RCA4	☑✲	☑✲	☑✲	☑✲	☑✲	☑✲
ICHEC-EC-EARTH	r3i1p1	SMHI-RCA4	☑	☑	☑	☑	☑	☑
MOHC-HadGEM2-ES	r1i1p1	CLMcom-CCLM4-8-17	☑	☑	☑	☑	☑	☑
MOHC-HadGEM2-ES	r1i1p1	DMI-HIRHAM5	☑	☑	☑	☑	☑	☑
MOHC-HadGEM2-ES	r1i1p1	KNMI-RACMO22E	☑✲	☑✲	☑✲	☑✲	☑✲	☑✲
MOHC-HadGEM2-ES	r1i1p1	SMHI-RCA4	☑✲	☑✲	☑✲	☑✲	☑✲	☑✲
MOHC-HadGEM2-ES	r1i1p1	GERICS-REMO2015	☑✲	☑✲	☑✲	☑✲	☑✲	☑✲
MOHC-HadGEM2-ES	r1i1p1	ICTP-RegCM4-6	☑✲	☑✲	☑✲	☑✲	☑✲	☑✲
MOHC-HadGEM2-ES	r1i1p1	UHOH-WRF361H	☑	☑	☑		☑	
MOHC-HadGEM2-ES	r1i1p1	IPSL-WRF381P	☑	☑	☑	☑	☑	☑
MOHC-HadGEM2-ES	r1i1p1	CNRM-ALADIN63	☑	☑	☑	☑	☑	☑
IPSL-IPSL-CM5A-MR	r1i1p1	SMHI-RCA4	☑	☑	☑	☑	☑	☑
IPSL-IPSL-CM5A-MR	r1i1p1	IPSL-WRF381P	☑	☑	☑	☑	☑	☑
IPSL-IPSL-CM5A-MR	r1i1p1	KNMI-RACMO22E	☑	☑	☑	☑	☑	☑

MIROC-MIROC5	r1i1p1	CLMcom-CCLM4-8-17	☑✲	☑✲	☑✲	☑✲	☑✲	☑✲
MIROC-MIROC5	r1i1p1	GERICS-REMO2015	☑✲	☑✲	☑✲	☑✲	☑✲	☑✲
MPI-M-MPI-ESM-LR	r1i1p1	CLMcom-CCLM4-8-17	☑✲	☑✲	☑✲	☑	☑	☑✲
MPI-M-MPI-ESM-LR	r1i1p1	KNMI-RACMO22E	☑	☑	☑	☑	☑	☑
MPI-M-MPI-ESM-LR	r1i1p1	SMHI-RCA4	☑	☑	☑	☑✲	☑✲	☑✲
MPI-M-MPI-ESM-LR	r1i1p1	MPI-CSC-REMO2009	☑✲	☑✲	☑✲	☑✲	☑✲	☑✲
MPI-M-MPI-ESM-LR	r1i1p1	ICTP-RegCM4-6	☑✲	☑✲	☑✲	☑	☑	☑
MPI-M-MPI-ESM-LR	r1i1p1	UHOH-WRF361H	☑✲	☑✲	☑✲		☑	
MPI-M-MPI-ESM-LR	r1i1p1	CLMcom-ETH-COSMO-crCLIM-v1-1	☑	☑	☑	☑	☑	☑
MPI-M-MPI-ESM-LR	r2i1p1	MPI-CSC-REMO2009	☑✲	☑✲	☑✲	☑✲	☑✲	☑✲
MPI-M-MPI-ESM-LR	r2i1p1	CLMcom-ETH-COSMO-crCLIM-v1-1	☑	☑	☑	☑	☑	☑
MPI-M-MPI-ESM-LR	r3i1p1	SMHI-RCA4	☑✲	☑✲	☑✲	☑	☑	☑
MPI-M-MPI-ESM-LR	r3i1p1	GERICS-REMO2015	☑✲	☑✲	☑✲	☑	☑	☑
MPI-M-MPI-ESM-LR	r3i1p1	CLMcom-ETH-COSMO-crCLIM-v1-1	☑	☑	☑	☑	☑	☑
NCC-NorESM1-M	r1i1p1	DMI-HIRHAM5	☑	☑	☑	☑	☑	☑
NCC-NorESM1-M	r1i1p1	KNMI-RACMO22E	☑	☑	☑	☑	☑	☑
NCC-NorESM1-M	r1i1p1	GERICS-REMO2015	☑	☑	☑	☑✲	☑✲	☑✲
NCC-NorESM1-M	r1i1p1	SMHI-RCA4	☑	☑	☑	☑✲	☑✲	☑✲
NCC-NorESM1-M	r1i1p1	IPSL-WRF381P	☑	☑	☑	☑	☑	☑
NCC-NorESM1-M	r1i1p1	CLMcom-ETH-COSMO-crCLIM-v1-1	☑	☑	☑	☑	☑	☑

Table 2:

CMIP5 models and their corresponding variant label used for this report (☑rcp8.5, ✳=rcp2.6)

CMIP5	**Variant**	**tas**	**tasmax**	**tasmin**	**q**	**pr**	**rsds**
CanESM2	r1i1p1	☑	☑	☑	☑✳	☑	☑✳
CNRM-CM5	r1i1p1	☑✳	☑✳	☑✳	☑✳	☑✳	☑✳
EC-EARTH	r12i1p1	☑✳	☑✳	☑✳		☑✳	☑
EC-EARTH	r3i1p1	☑	☑	☑		☑	
EC-EARTH	r1i1p1	☑	☑	☑		☑	☑
HadGEM2-ES	r1i1p1	☑✳	☑✳	☑✳	☑✳	☑✳	☑✳
IPSL-CM5A-MR	r1i1p1	☑	☑	☑	☑✳	☑	☑✳
MIROC5	r1i1p1	☑✳	☑✳	☑✳	☑✳	☑✳	☑✳
MPI-ESM-LR	r1i1p1	☑✳	☑✳	☑✳		☑✳	☑✳
MPI-ESM-LR	r2i1p1	☑✳	☑✳	☑✳		☑✳	☑✳
MPI-ESM-LR	r3i1p1	☑	☑	☑		☑	☑✳
NorESM1-M	r1i1p1	☑✳	☑✳	☑✳	☑	☑✳	☑✳

Table 3:

CMIP6 models and their corresponding variant label used for this report [☑=ssp585, ✳=ssp126].

CMIP6	Variant	tas	tasmax	tasmin	q	pr	rsds
BCC-CSM2-MR	r1i1p1f1	☑✻	☑✻	☑✻	☑✻	☑✻	☑✻
CNRM-CM6-1	r1i1p1f2	☑✻	☑✻	☑✻	☑	☑✻	☑✻
CNRM-ESM2-1	r1i1p1f2	☑✻	☑✻	☑✻	☑✻	☑✻	☑✻
CanESM5	r1i1p1f1	☑✻	☑✻	☑✻	☑✻	☑✻	☑✻
EC-Earth3	r1i1p1f1	☑✻	☑✻	☑✻	☑✻	☑✻	☑✻
EC-Earth3-Veg	r1i1p1f1	☑✻	☑✻	☑✻	☑✻	☑✻	☑✻
GFDL-CM4	r1i1p1f1	☑	☑	☑	☑	☑	☑
IPSL-CM6A-LR	r1i1p1f1	☑✻	☑✻	☑✻	☑	☑✻	☑✻
MIROC6	r1i1p1f1	☑✻	☑✻	☑✻		☑✻	☑✻
MRI-ESM2-0	r1i1p1f1	☑✻	☑✻	☑✻	☑✻	☑✻	☑✻
NESM3	r1i1p1f1	☑✻	☑✻	☑✻		☑✻	☑✻
UKESM1-0-LL	r1i1p1f2	☑✻	☑✻	☑✻	☑✻	☑✻	☑✻

Table 4:
Diagnostics and climate indices used in this study.

Variable	Analyzed Period	Description
Daily mean temperature (TAS)	Year, DJF, JJA, SON, MAM	Yearly and seasonal mean temperature from daily mean temperature °C

Daily max temperature (TASMAX)	Year, DJF, JJA, SON, MAM	Yearly or seasonal mean of daily maximum temperature, ° C
Daily min temperature (TASMIN)	Year, DJF, JJA, SON, MAM	Yearly or seasonal mean of daily minimum temperature, °C
TXx (yearly max temperature)	Year	Yearly maximum of daily maximum temperature, °C
TNn (yearly min temperature)	Year	Yearly minimum of daily minimum temperature, °C
#days/year TX>35°C (TX35)	Year	Number of days per year with maximum temperature over 35 °C
#days/year TX>40°C (TX40)	Year	Number of days per year with maximum temperature over 40 °C
#days wet bulb globe temperature>31°C (WBGTs31)	Year	Number of days per year with wet bulb globe temperature (WBGT) larger than 31°C
#Frost days/year (FD)	Year	Number of days per year with minimum temperature below 0°C
Length of frost-free period (LFFP)	Year	Maximum continuous number of days per year where daily minimum temperature is above 0 °C (units= days). (McCabe et al., 2015)
Growing degree days > 5°C (GDD)	Year	The accumulated sum of the difference between daily mean temperature and the threshold (5 °C) (when higher than the threshold) over the April-September months (units= degree days) (McCabe et al., 2015; Ruosteenoja et al., 2016; Spinoni et

		al., 2015)
Heating degree day > 15.5 (HDD)	Year	Heating degree days, threshold (Tb) = 15.5°C, following Spinoni et al., (2015), which uses the mean (TM), maximum (TX) and minimum (TN) daily temperature as follows (units= degree days): $HDD_i = \begin{cases} T_b - T_M \\ \frac{T_b - T_N}{2} - \frac{T_X - T_b}{4} \\ \frac{T_b - T_N}{4} \\ 0 \end{cases} \quad if \quad \begin{cases} T_X \le T_b \\ T_M \le T_b < T_X \\ T_N \le T_b < T_M \\ T_N \ge T_b \end{cases}$ Then $HDD = \sum_{i=1}^{365} HDD_i$ We use all months of the year
Cooling degree day > 22°C (CDD)	Year	C ooling degree days, threshold (Tb) = 22 °C, following Spinoni et al., (2015), which uses the mean (TM), maximum (TX) and minimum (TN) daily temperature as follows (units= degree days): $CDD_i = \begin{cases} 0 \\ \frac{T_X - T_b}{4} \\ \frac{T_X - T_b}{2} - \frac{T_b - T_N}{4} \\ T_M - T_b \end{cases} \quad if \quad \begin{cases} T_X \le T_b \\ T_M \le T_b < T_X \\ T_N \le T_b < T_M \\ T_N \ge T_b \end{cases}$ Then $CDD = \sum_{i=1}^{365} CDD_i$ We use all months of the year
Daily precipitation	Year, DJF, JJA, SON, MAM	

amount (PR)		
SDII	Year	Simple Daily Intensity Index (Units= mm/day)
RX1day	Year	Highest 1-day precipitation amount (Units= mm/day)
RX5day	Year	Highest 5-days precipitation amount (Units= mm/5days)
P99	Year	Days with RR>99th percentile of daily amounts (extremely wet days) Units: days
CDD_pr	Year	Mean Consecutive Dry Days per year. Units=number of days
Drought Frequency (DF)	Year	Drought frequency change per decade, based on a Standardized Precipitation Index (SPI) computed for a six-month accumulation period
Downward surface solar radiation (RSDS)	Year	rsds variable

Figures

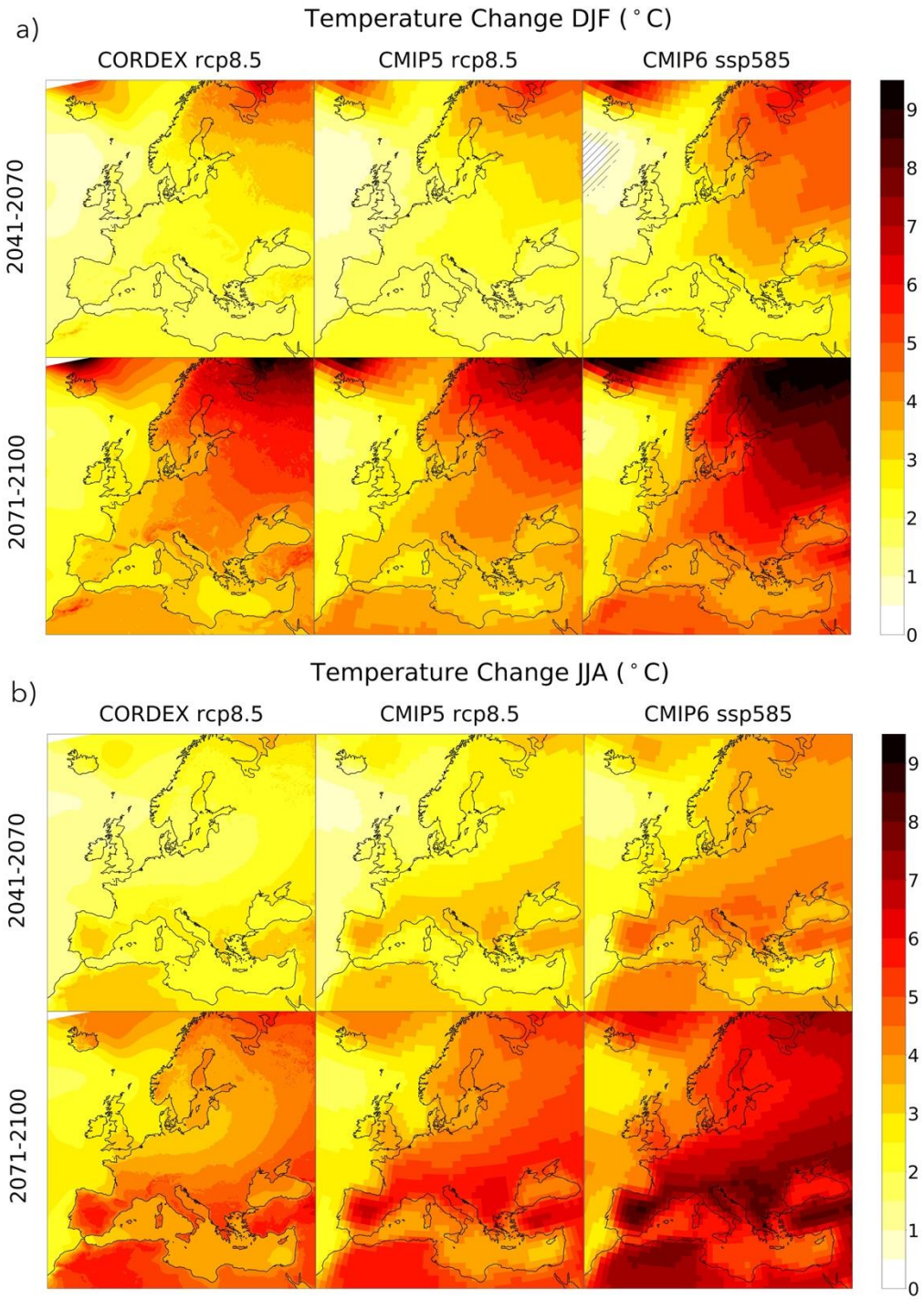

Fig. 1 – Seasonal mean temperature ensemble mean changes (DJF (a) and JJA (b)) for EURO - CORDEX (55 simulations), CMIP5 (12 simulations) and CMIP6 (12 simulations) for 2041-2070 (Mid future) and 2071-2100 (Far future) relative to 1981- 2010 (Units: degrees). Dashed lines cover areas where changes are not significant at the 95% confidence level (Student's ttest).

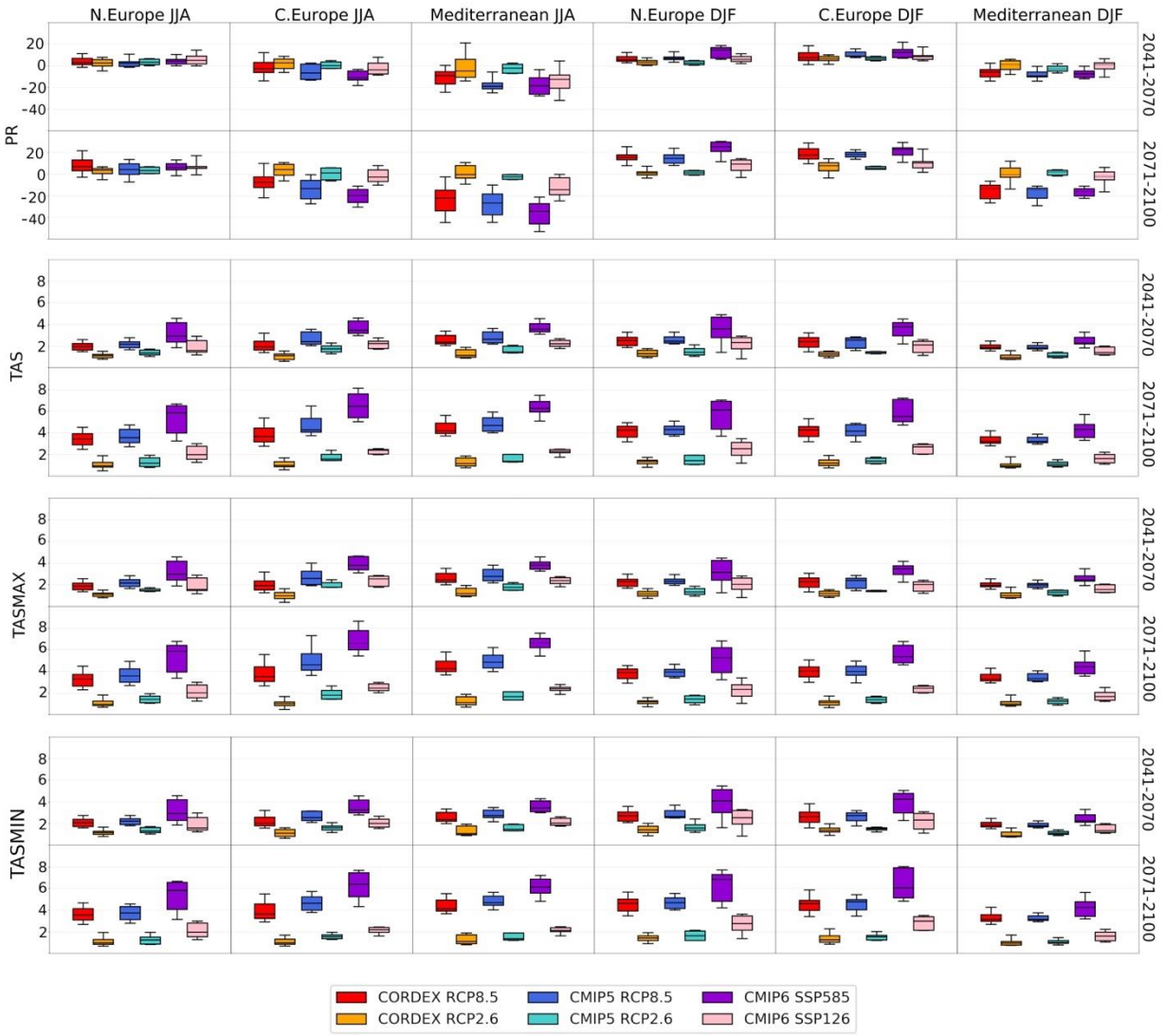

Fig. 2 – Summer (JJA) and Winter (DJF) daily precipitation (Units=percentage) and temperature (mean temperature *tas*, minimum temperature *tasmin*, and maximum temperature *tasmax*, Units= degrees) changes of 2041-2070 (Mid) and 2071-2100 (Far) relative to 1981-2010 for the three European SREX regions (Northern Europe, Central Europe, Mediterranean region). The colors indicate different ensembles (CORDEX (55 simulations), CMIP5 (12 simulations) and CMIP6 (12 simulations)) under different scenarios (rcp85, rcp26, ssp585 and ssp126). Colored bars represent the model spread between the 25th and 75th percentiles, while the black bars indicate the 5th, the 50th and 95th percentiles.

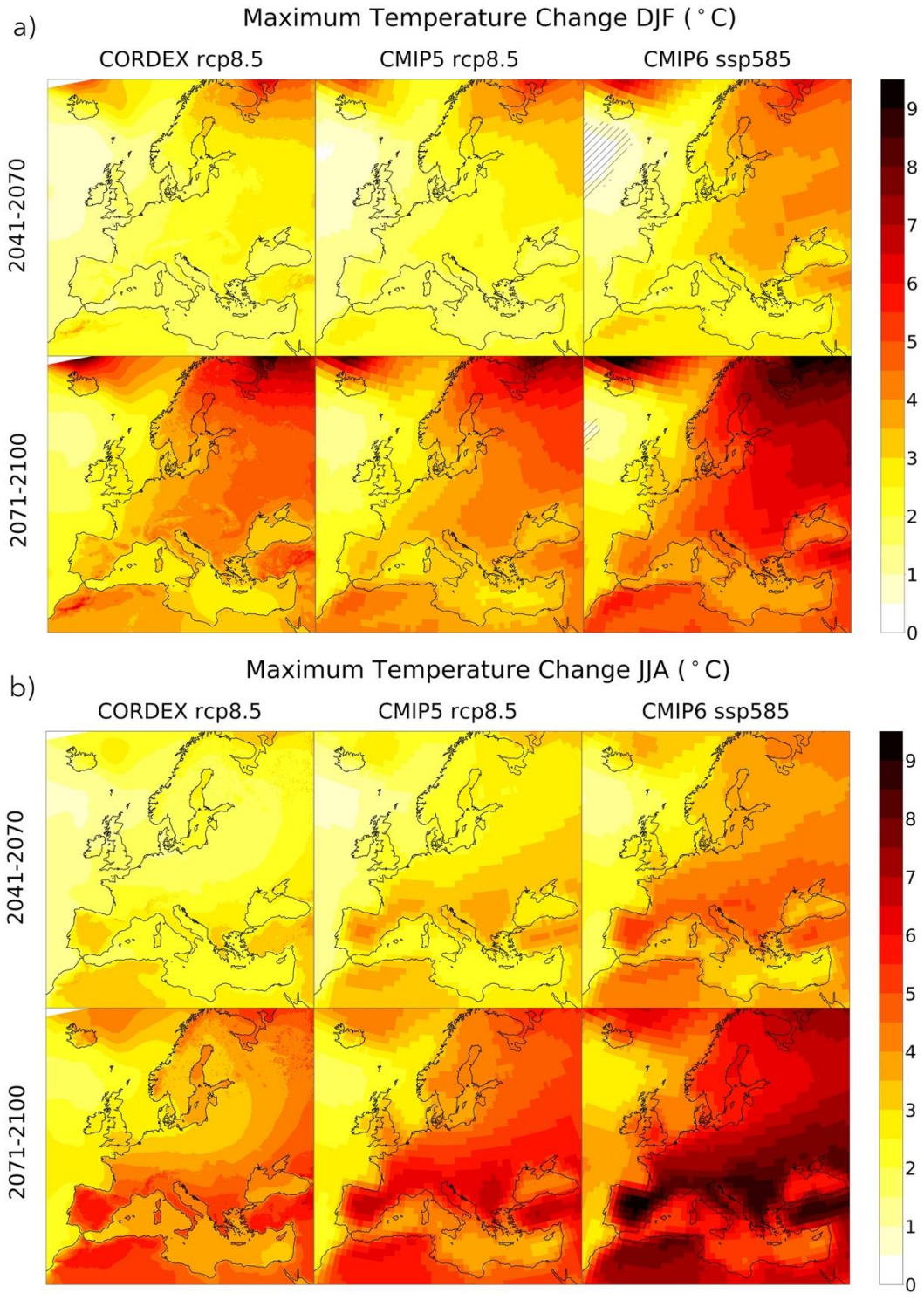

Fig. 3 – As in Fig.1 for seasonal maximum temperature ensemble changes (DJF (a) and JJA (b)) (Units: degrees). Dashed lines cover areas where changes are not significant at the 95% confidence level (Student's ttest).

863

864

865

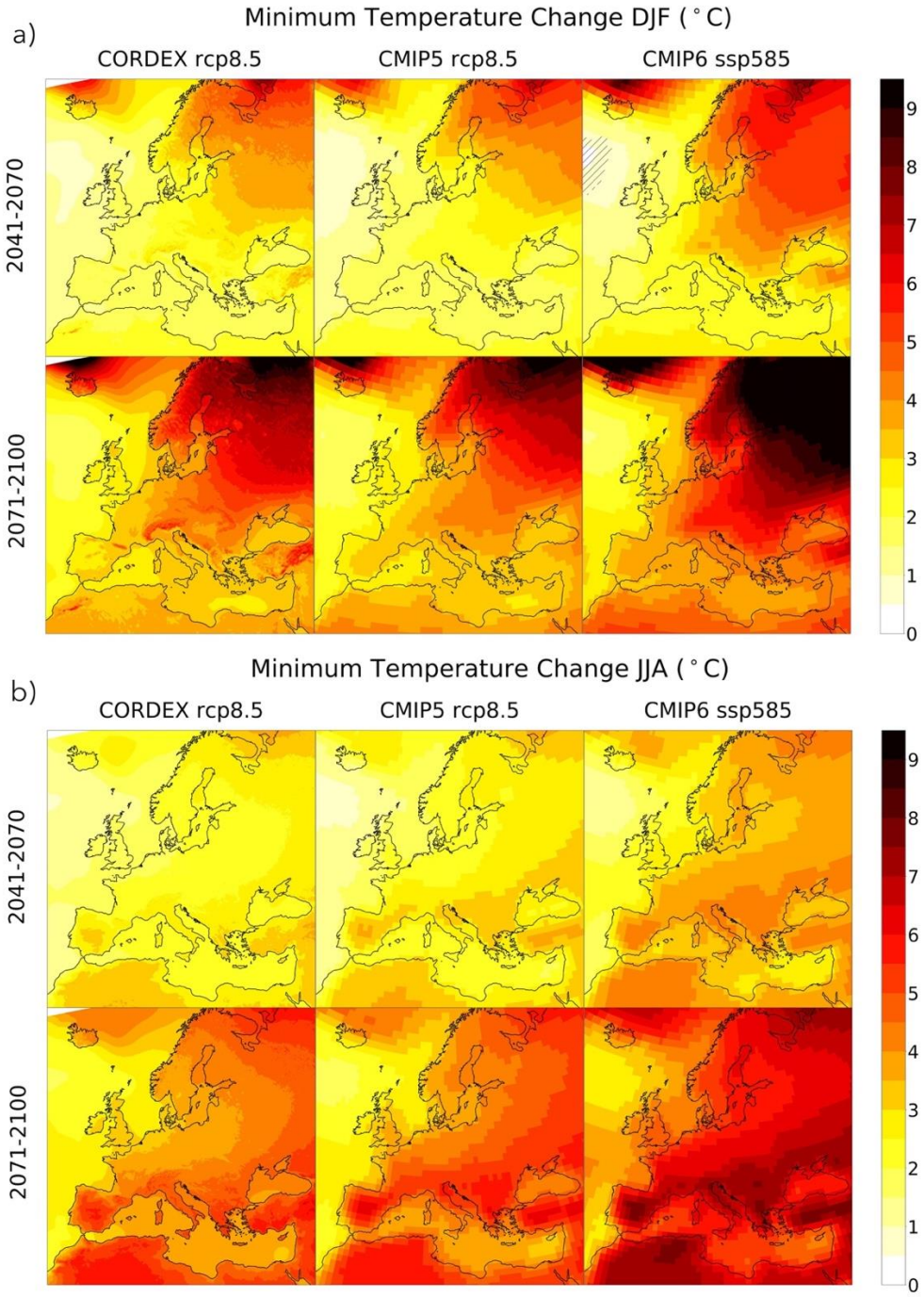

866

867 Fig. 4 – As in Fig.1 for seasonal minimum temperature ensemble changes (DJF (a) and JJA (b))
868 (Units: degrees). Dashed lines cover areas where changes are not significant at the 95%
869 confidence level (Student's ttest).

870

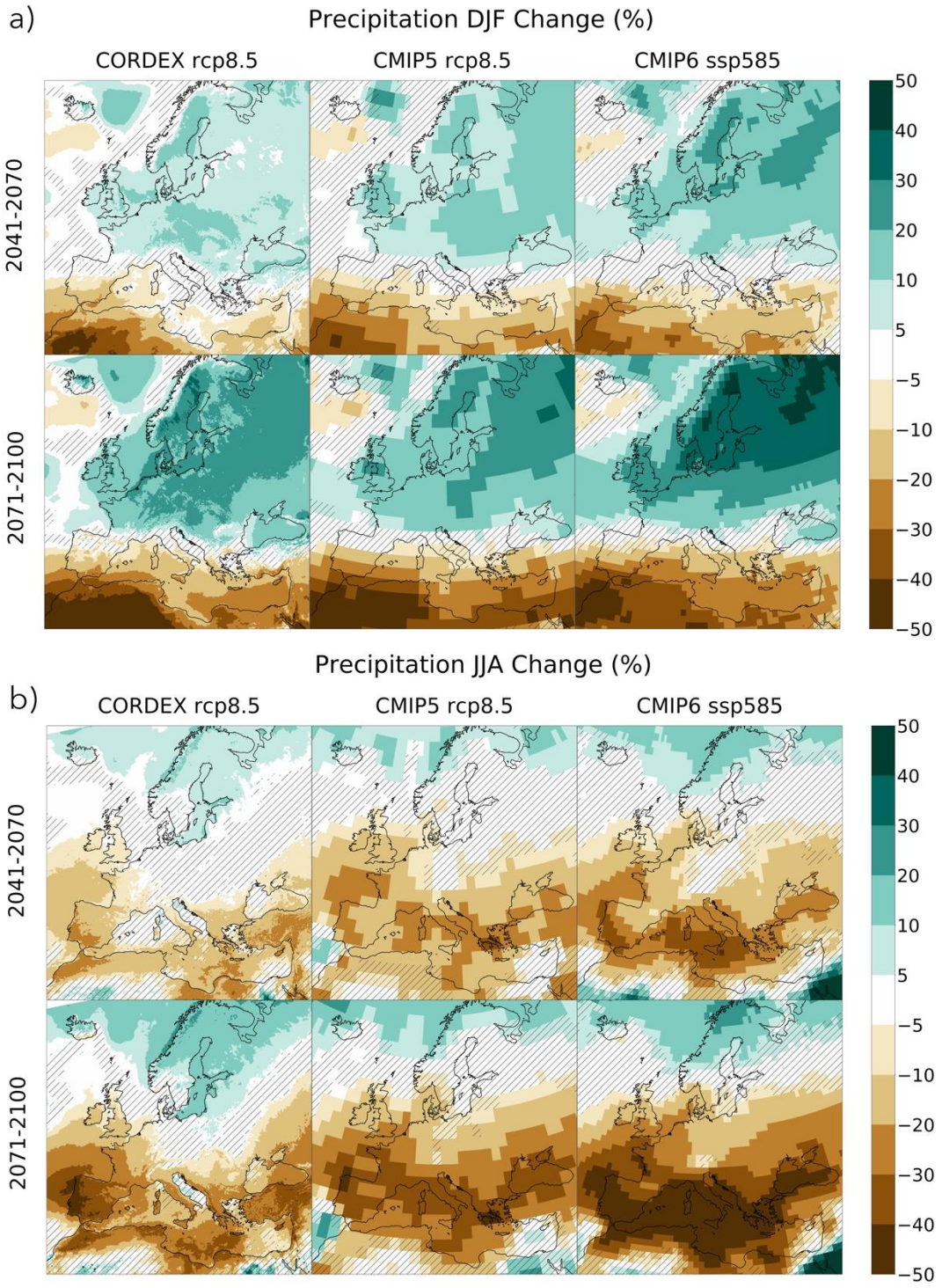

871

872 Fig. 5 – As in Fig.1 for seasonal precipitation ensemble changes (DJF (a) and JJA (b)) (Units:
873 percentage). Dashed lines cover areas where changes are not significant at the 95% confidence
874 level (Student's t test).

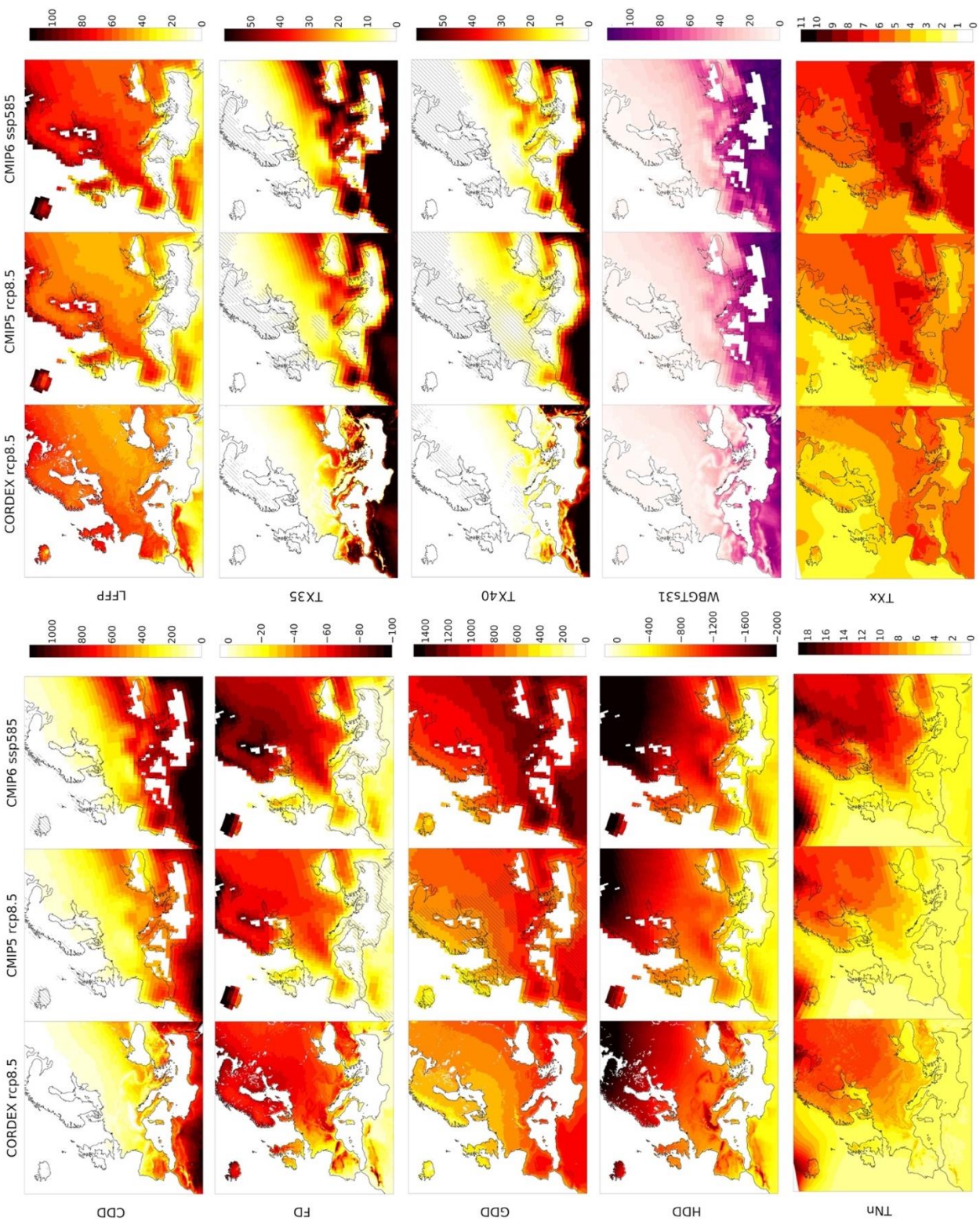
CMIP6 ssp585
CMIP5 rcp8.5
CORDEX rcp8.5
TXx
WBGTs31
TX40
TX35
LFFP
TNn
HDD
GDD
FD
CDD

878 Fig. 6 - Changes of the following indices: Cooling degree days > 22°C change (CDD, Units:
879 degree days derived over the whole year), Frost days (FD, Units: number of days per year),
880 Growing degree days > 5 °C (GDD, Units: degree days), Heating degree days (HDD, Units:
881 degree days), Length of Frost-Free Period change (LFFP, Units: days), number of days per year
882 with maximum temperature over 35 and 40 degrees °C. (TX30 and TX40, Units: days per year),
883 number of yearly events with wet bulb globe temperature greater than 31 °C. (WBGTs31, Units:
884 number of events per year). Results are shown for EUROuro-CORDEX (55 simulations), CMIP5
885 (12 simulations) and CMIP6 (12 simulations) for 2071-2100 (Far future) relative to 1981-2010.
886 Dashed lines cover areas where changes are not significant at the 95% confidence level
887 (Student's ttest).

888

889

890

891

892

893

894

895

896

897

898

899

900

901

902

903

904

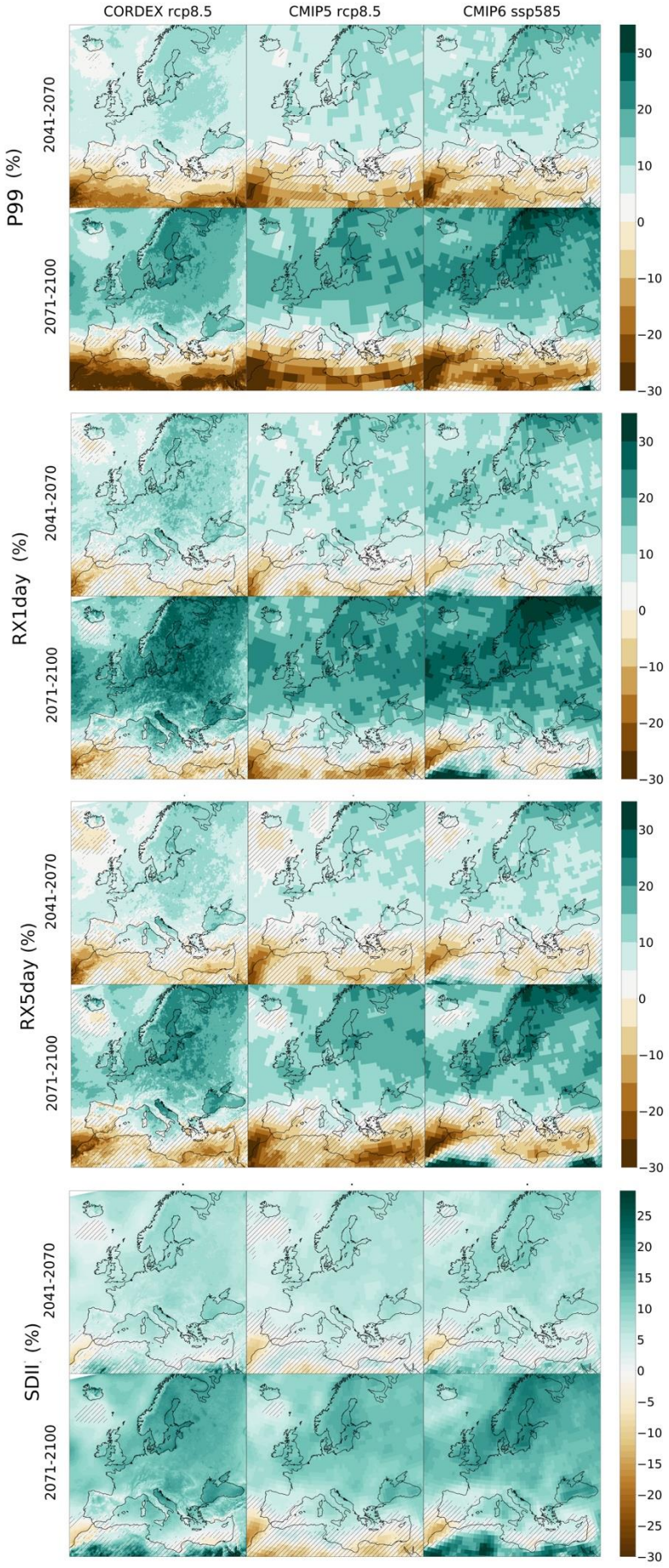
CORDEX rcp8.5
CMIP5 rcp8.5
CMIP6 ssp585
P99 (%)
RX1day (%)
RX5day (%)
SDII (%)
2041-2070
2071-2100
30
20
10
0
−10
−20
−30
25
15
5
−5
−15
−25

905

Fig.7 – As in Fig. 1 for annual changes of the following indices: the yearly 99th percentile of daily precipitation ensemble changes (Units: percentage), the maximum 1-day precipitation changes (RX1day) (Units: percentage), the maximum 5-days precipitation changes (RX5day) (Units: percentage) and the simple daily intensity precipitation index (SDII) (Units: percentage). Dashed lines cover areas where changes are not significant at the 95% confidence level (Student's ttest).

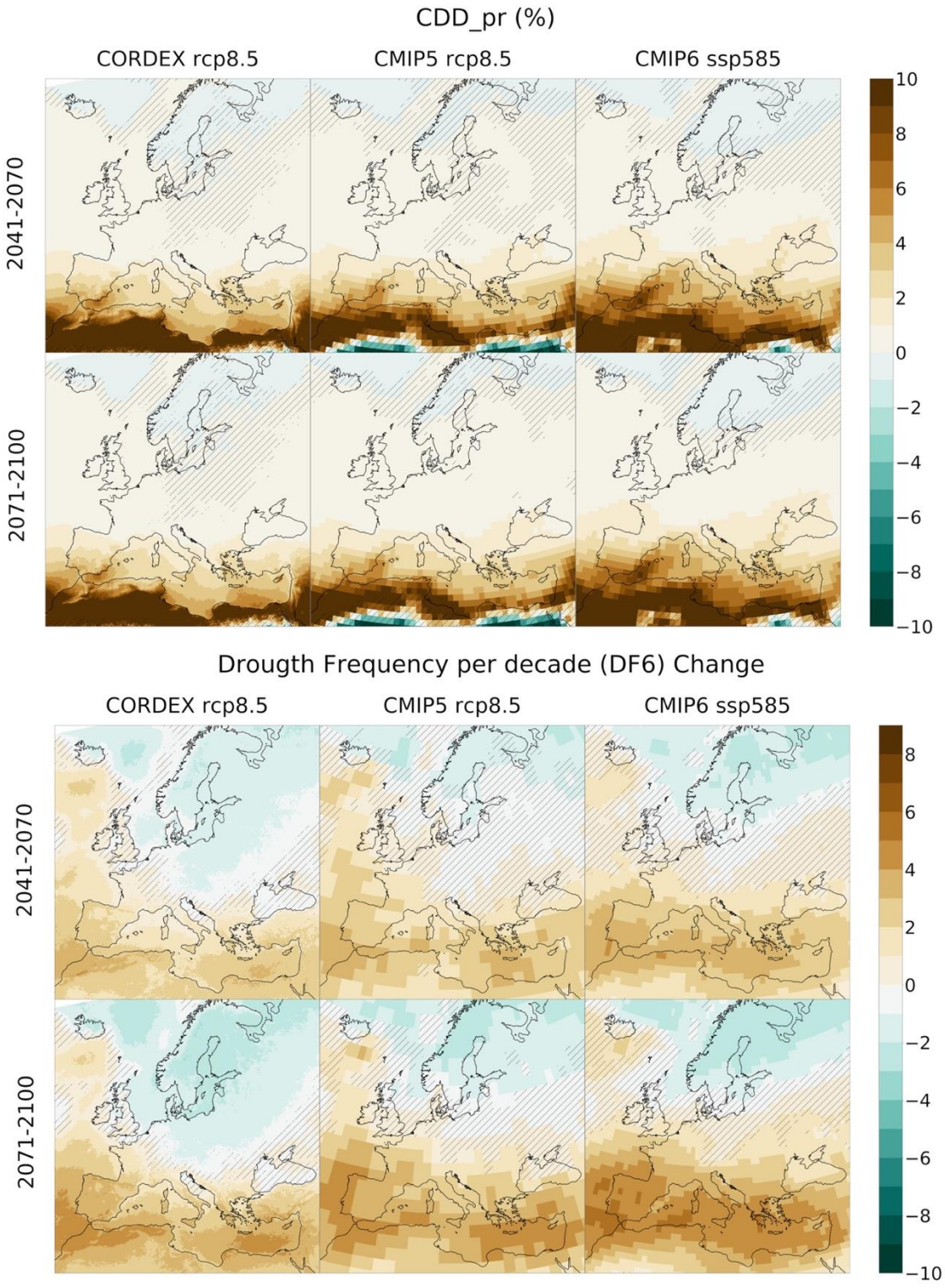

Fig. 8 - As in Fig.1 for changes of the Consecutive Dry Day Index (CDD, Units: days) and of the Drought frequency per decade, based on a SPI-6 months (DF6, Units: events per decade). Dashed lines cover areas where changes are not significant at the 95% confidence level (Student's t test).

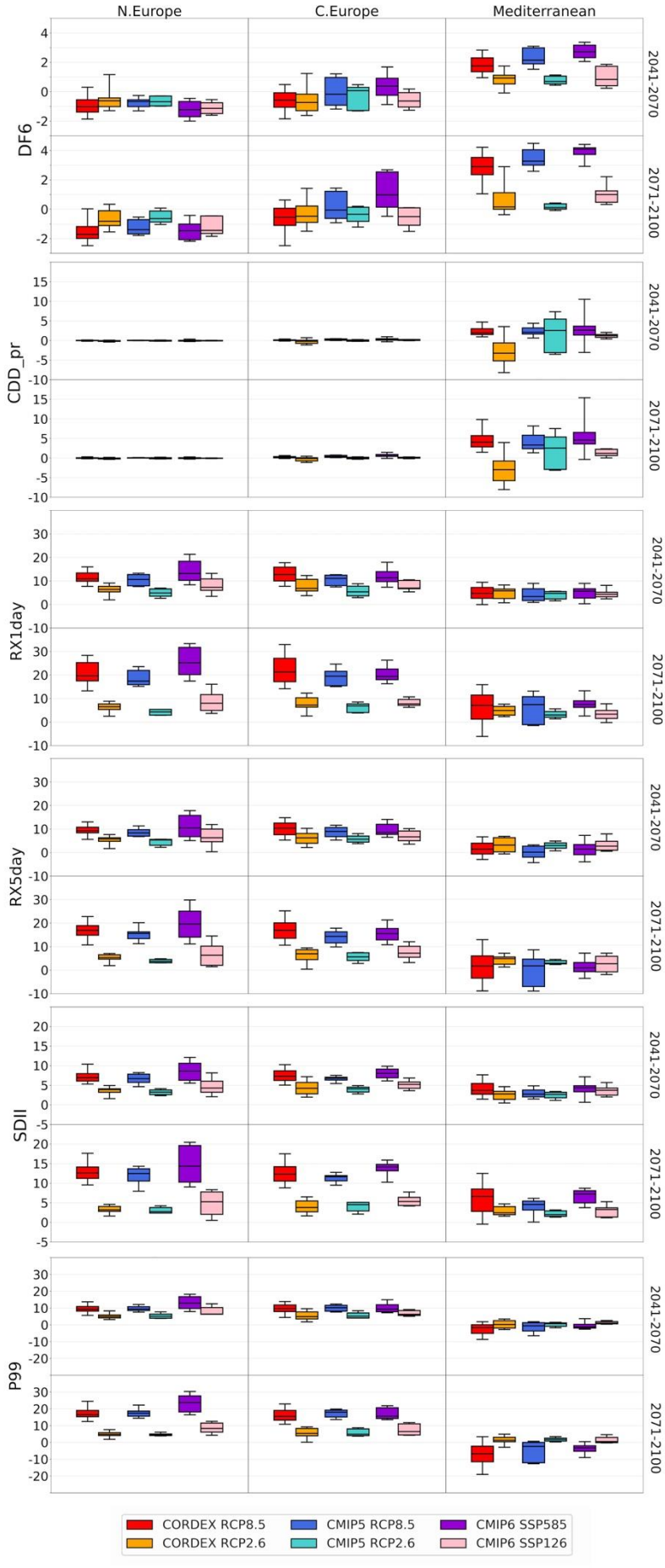
N.Europe
C.Europe
Mediterranean
DF6
CDD_pr
RX1day
RX5day
SDII
P99
2041-2070
2071-2100
CORDEX RCP8.5
CORDEX RCP2.6
CMIP5 RCP8.5
CMIP5 RCP2.6
CMIP6 SSP585
CMIP6 SSP126

922

Fig. 9 – As in Fig. 2 for the following indices: the Drought Frequency (DF6, Units=events per decade), the number of Consecutive Dry Days change (CDD, Units=days), the Maximum 1-day precipitation changes (RX1day, Units: percentage), the Maximum 5-days precipitation changes (RX5day, Units: percentage) and the Surface Downwelling Shortwave radiation (Units: W/m^2).

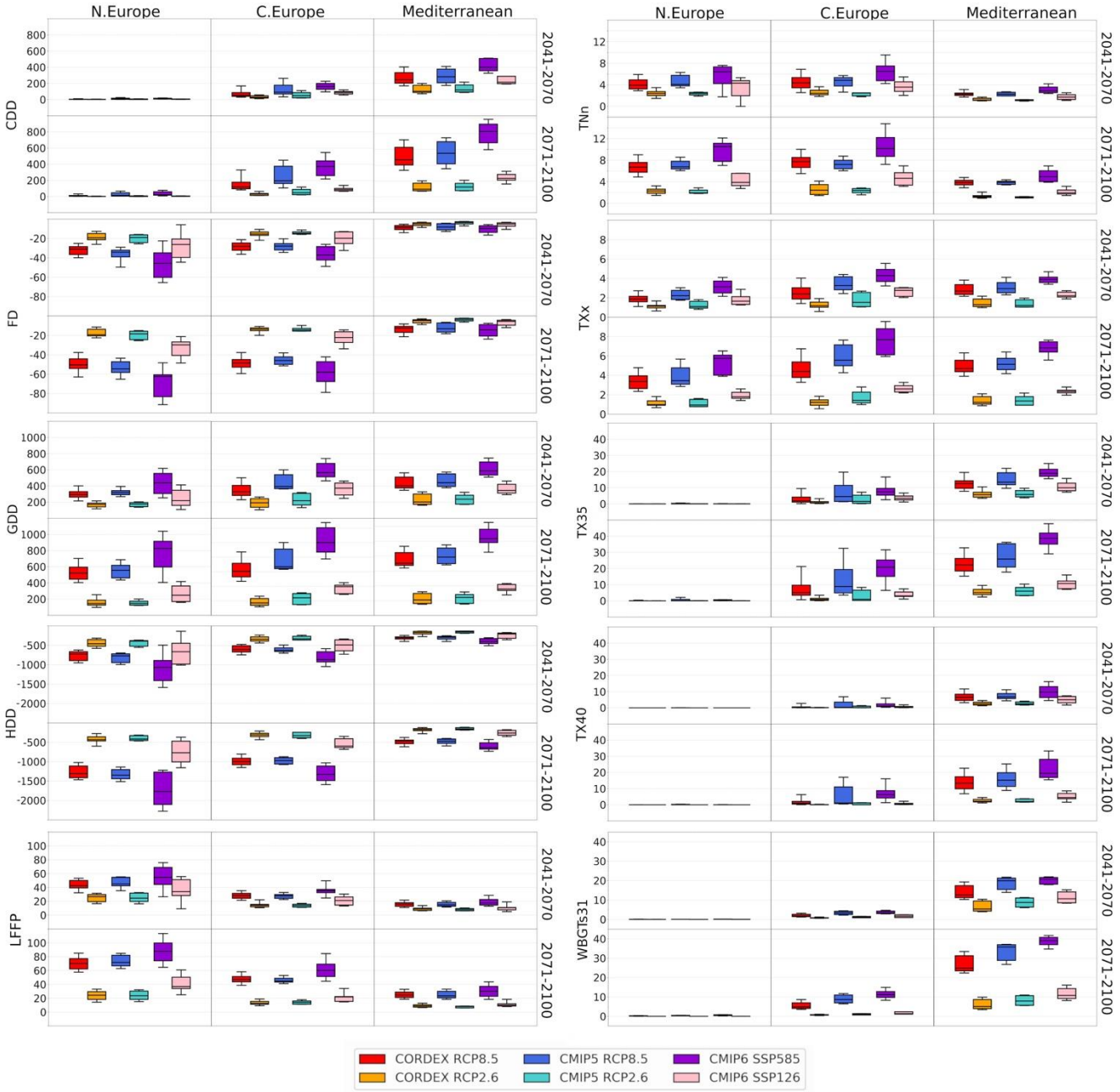

931

932

933 Fig. 10. As in Fig. 2 for the temperature climate indices: the Cooling Degree Days (CDD, Units:
934 degree days), the Frost Days changes (FD, Units = days per year), the Growing Degree Days
935 (TX35, TX40, Units =degree days), the Heating Degree Days (HDD, Units: degree days), the
936 Length of Frost Free Periods changes (LFFP, Units = days), the yearly maximum of daily
937 minimum temperature (TNn, Units= °C), the yearly maximum of daily maximum temperature
938 (TXx, Units= °C), the number of days per year with maximum temperature over 35 and 40

939 degrees °C (TX35 and TX40, Units = days per year) and the wet bulb globe temperature greater
940 than 31 °C (WBGT, Units = number of events).

941

942

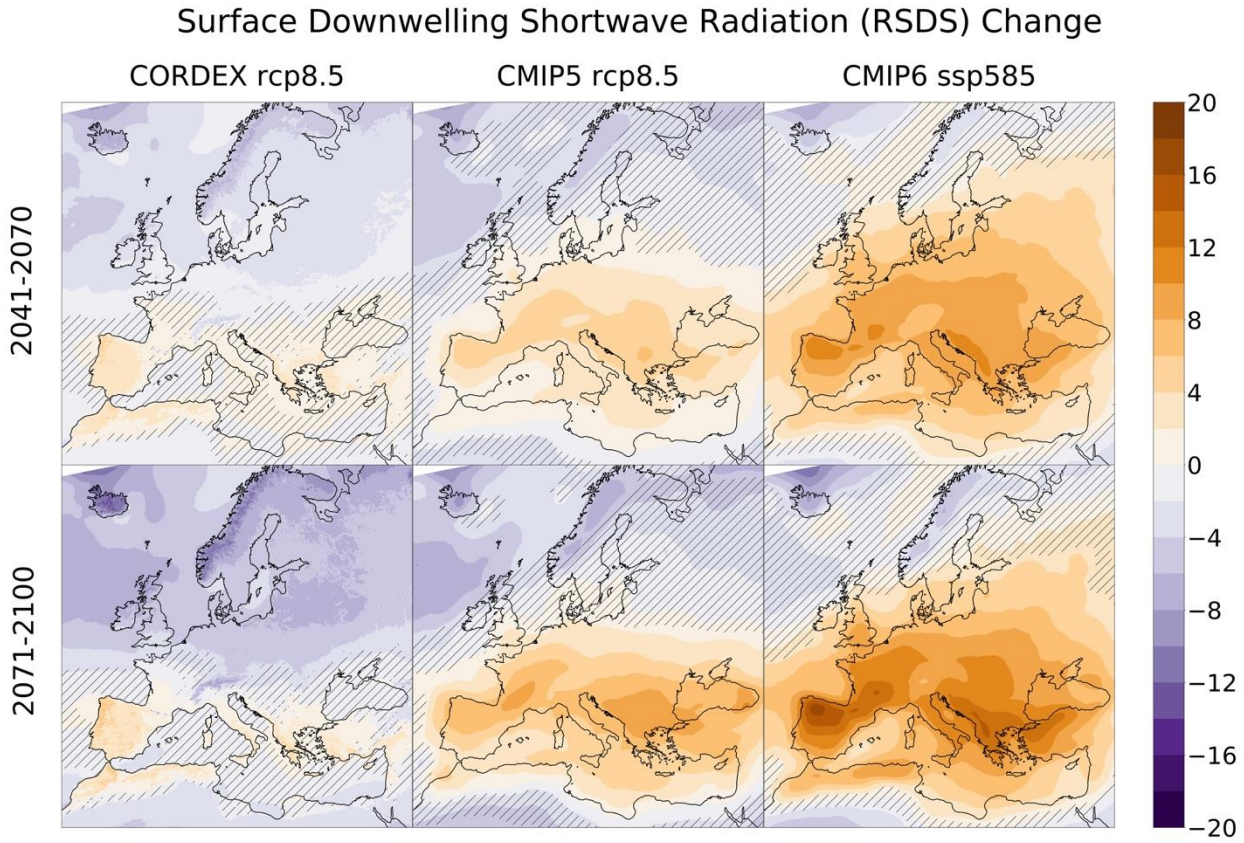

943
944 Fig. 11 – As in Fig.1 for changes in the Surface Downwelling Shortwave Radiation (Units:
945 W/m^2). Dashed lines cover areas where changes are not significant at the 95% confidence level
946 (Student's t test).

947

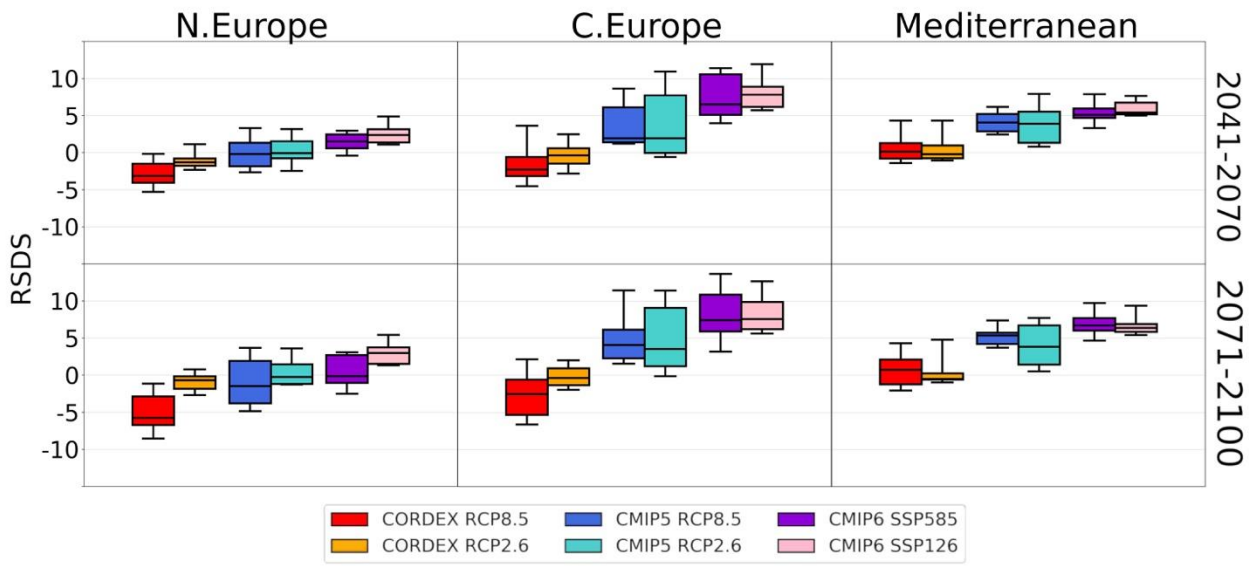

Fig. 12 – As in Fig. 2 for the Surface Downwelling Shortwave radiation (Units: W/m2)